Tectonic record and gold mineralization in the central part of the Neoproterozoic Keraf suture, Gabgaba district, NE Sudan

Julien Perret, Julien Feneyrol, Aurélien Eglinger, Anne-Sylvie André-Mayer, Célestine Berthier, Aomar Ennaciri, Rémi Bosc

HAL Id: hal-03226974
https://hal.science/hal-03226974

Submitted on 16 May 2021

Tectonic record and gold mineralization in the central part of the Neoproterozoic Keraf suture, Gabgaba district, NE Sudan

Julien Perret[1,2,*], Julien Feneyrol[1], Aurélien Eglinger[2], Anne-Sylvie André-Mayer[2], Célestine Berthier[2], Aomar Ennaciri[3], Rémi Bosc[1]

[1] Arethuse Geology EURL, BP 80017, Latitude Arbois, 1060 rue René Descartes, 13290 Les Milles, France

[2] GeoRessources, Université de Lorraine, CNRS, 54000 Nancy, France

[3] Managem, BP5199, Twin Center, Tour A, Boulevard Zerktouni, Casablanca, Maroc

Abstract

The central Keraf suture recorded complex lithospheric-scale deformation associated with the formation of the Neoproterozoic Arabian-Nubian shield and hosts the WG03, Central Zone and UTM gold deposits, Gabgaba district, northeastern Sudan. This study aims at (i) unravelling the tectonic history recorded by the central Keraf suture and (ii) interpreting the spatial and genetic relationships between structural setting and gold mineralization. To this end, we coupled field petrographic observations and structural measurements made along a 50 km-long geological cross-section through the Gabgaba district with macroscopic and microscopic description of mineralized structures.

The structural setting of the central Keraf suture is dominated by progressive deformation, from ductile D_{1a} Keraf thrusting to ductile-brittle D_{1b} sinistral shearing in a prolonged northwest-orientated convergence regime. A first mineralization event, leading to a minor gold endowment, relates to magmatic accretion pre-dating D_{1a} Keraf suturing. The second gold episode is characterized by ore veining as a response to progressive late collisional D_{1b} Keraf strike-slip shearing and may be classified as orogenic gold. Most of the gold budget of the Gabgaba district formed at this stage.

In summary, the central Keraf suture exemplifies that the Arabian-Nubian shield contains significant polyphase gold mineralization along lithospheric-scale structures. These structures may record a complex tectonic evolution from magmatic accretion to collision, with a strong structural control on gold endowment.

Keywords

1. Introduction

Archean to Phanerozoic orogenic gold deposits are systematically associated with crustal to lithospheric-scale structures along accretionary- and collision-type convergent margins (*e.g.,* Kerrich and Wyman, 1990; Goldfarb et al., 2001, 2005; Groves et al., 2003, 2018, 2019; Weinberg et al., 2004; Bierlein et al., 2006; Eglinger et al., 2017). Lithospheric-scale transcurrent shear zones may develop at the boundary between litho-tectonic blocks or terranes and play a critical role as fluid and magma pathways (*e.g.,* Kerrich and Wyman, 1990; Sawkins, 1990; Weinberg et al., 2004, 2005; Blewett et al., 2010; Mole et al., 2019). Although these transcurrent shear zones mostly result from the syn- to late convergent stage, some record a much more complex polyphase deformation history starting earlier in the orogenic cycle with the formation of suture zones (*e.g.,* Daigneault et al., 2002; Weinberg et al., 2004; Feybesse et al., 2006). These complex, transcurrent, lithospheric-scale structures are known to host orogenic gold deposits in world-class gold provinces, such as the Boulder-Lefroy fault system in the Archean Yilgarn craton (*e.g.,* Weinberg et al., 2005; Mueller et al., 2020; Mueller, 2020), the Cadillac-Larder Lake fault zone in the Archean Abitibi subprovince (*e.g.,* Rabeau et al., 2013; Simard et al., 2013; Bedeaux et al., 2017) or the Markoye shear zone in the Paleoproterozoic West African craton (*e.g.,* Fontaine et al., 2017; Goldfarb et al., 2017). Several gold events may then occur from the magmatic arc accretion to the late orogenic periods (*e.g.,* Simard et al., 2013; Augustin et al., 2017; Eglinger et al., 2017, 2020; Le Mignot et al., 2017; Thébaud et al., 2020; Masurel et al., 2021). These gold-mineralized shear zones therefore have the potential to provide important relationships between tectonic processes and gold endowment through time.

The Arabian-Nubian shield (ANS; Fig. 1a, b) constitutes the main Neoproterozoic gold province worldwide (Johnson et al., 2017). ANS deposits are mostly classified as orogenic gold occurrences preferentially hosted by major shear zones (*e.g.,* Elsamani et al., 2001; Botros, 2002, 2004; Helmy et al., 2004; El Kazzaz, 2012; Osman, 2014; Helmy

and Zoheir, 2015; Khalil et al., 2016; Fawzy, 2017; Zoheir et al., 2019a, 2019b, 2019c), including the Keraf shear zone (KSZ) (Johnson et al., 2017). The KSZ is mapped in northeastern Sudan and southeastern Egypt, and overprints the ~500 km-long, ~70 km-wide, north-striking ophiolite-decorated Keraf suture (KS) which is rooted deep into the lithosphere (Almond and Ahmed, 1987; Abdelrahman, 1993; Abdelsalam et al., 1995; Abdelsalam and Stern, 1996a; Ahmed Suliman, 2000). The KS is divided in the northern, central and southern sections with distinct structural settings, despite it remains a poorly studied area with uncertain shape and boundaries (Fig. 1c). Second-order structures are known to host gold occurrences and deposits in the central KS, forming the Gabgaba gold district explored and exploited since 2009 by Manub, a subsidiary of the Moroccan mining group Managem Ltd. (Block 15 exploration license in Fig. 1c; Managem, 2011). Yet, the temporal and spatial relationships between the Gabgaba gold district deposits, *i.e.,* WG03, Central Zone and UTM -indicated and measured resources up to 1.659 Mozt Au, 438 kozt Au and 308 kozt Au in May 2013, respectively (Managem, 2014)- and the wider structural framework are scarcely documented (*e.g.,* Gaboury et al., 2020):

(i)   Central Zone and UTM deposits are located along a second-order structure, known as the *"West Corridor"* (Figs. 2, 3; Gaboury et al., 2020) but the interpretation of this structure as the western boundary of the central KS remains under debate (Fig. 2; Ahmed Suliman, 2000; Bailo et al., 2003; Abdelsalam et al., 1998; Gaboury et al., 2020).

(ii)   The WG03 deposit is located along another lower-order shear zone west of the *"West Corridor"* (Fig. 2), it remains thus unclear if the deposit is located within the KS and if WG03 gold endowment relates in any way to KS tectonics.

Much work therefore remains to be done to understand the gold endowment history related to the central KS tectonics and the Gabgaba district is well-suited to do so. Our study serves two purposes: (i) collecting field observations and structural measurements along the central section of the KS (Figs. 1c, 2, 3) to propose a revised tectonic history,

4

unifying previous models from the literature (*e.g.,* Abdelsalam et al., 1995, 1998; Ahmed Suliman, 2000); and (ii) linking the textural and structural characteristics of the known Gabgaba deposits with the wider tectonic framework, to interpret the spatial and genetic relationships between structural setting and gold mineralization. In order to address these two points, we realized a 50 km-long geological cross-section through the Gabgaba gold district and conducted a petrological-structural study of the WG03, Central Zone and UTM gold deposits.

2. Geological setting

The ANS is the northernmost part of the East African-Antarctic orogen (EAAO; Fig. 1a, b; Kröner, 1993; Stern, 1994; Kusky et al., 2003; Li et al., 2008; Seton et al., 2012; Fritz et al., 2013; Domeier and Torsvik, 2014; Merdith et al., 2017; Grenholm, 2019). Its formation resulted from the amalgamation and collision between terranes, formed by juvenile magmatic arc and ophiolite assemblages which are remnants of the subduction and obduction processes that completely consumed the Mozambique ocean in the northern EAAO (Fig. 1a; *e.g.,* Burke and Sengör, 1986; Johnson et al., 2011; Fritz et al., 2013 and references therein). It led to the formation of suture zones that are linear belt of intense deformation along which terranes join together and sometimes superimposed by crustal-scale shear zones (Chetty, 2017). The Keraf suture and shear zone is an example of such a composite orogenic belt (KS-KSZ; Fig. 1b).

The extent of the KS is limited to Egypt and Sudan as it represents the northern part of the Keraf-Kabus-Sekerr-Kinyiki suture (Fig. 1a) that stretches to Kenya southwards (Fig. 1a; Vearncombe, 1983; Burke and Sengör, 1986; Frisch and Pohl, 1986; Berhe, 1990; Abdelsalam and Dawoud, 1991; Ries et al., 1992; Mosley, 1993; Abdelsalam et al., 1998; Fritz et al., 2013). Keraf suturing consisted in arc-continent collision between Neoproterozoic juvenile magmatic arcs, and the Saharan meta-craton with consumption

of the Mozambique ocean lithosphere (Vail, 1983, 1985; Almond and Ahmed, 1987; Abdelsalam and Dawoud, 1991; Stern, 1994; Abdelsalam et al., 1995, 1998; Abdelsalam and Stern, 1996b; Abdelrahman et al., 2017).

The former presence of the Mozambique ocean in place of the current KS is underlined by the Keraf Pre-Tectonic Assemblage (KPTA; Fig. 1c). The KPTA gathers all the rocks exposed only in the KS zone and that are affected by Keraf thrusting and strike-slip shearing processes (Ahmed Suliman, 2000). It comprises pre-Neoproterozoic high- to medium-grade gneisses (Meinhold, 1979; Vail, 1979; Dawoud, 1980; Abdelrahman, 1993) and rock remnants related to different geodynamical settings such as magmatic arc and back-arc basin (Keraf ophiolitic mélange, volcanosedimentary sequences; *e.g.,* Schandelmeier et al., 1994; Stern, 1994; Abdelsalam et al., 1995; Abdelrahman et al., 2017) and passive continental margin (carbonate-rich and siliciclastic meta-sediments; *e.g.,* Stern et al., 1993). Following the Mozambique ocean expansion, the formation of the KS-KSZ recorded its closure and subsequent convergence:

(i)   Initial convergence and ocean closure occurred along a north-trending magmatic arc system that was active at *ca.* 800-750 Ma east to the Saharan meta-craton (Abdelsalam et al., 1998; Bailo et al., 2003). At the same time, west-trending aulacogen-like oceanic reentrants started to close along magmatic arcs as well, such as the one marked by the Atmur-Delgo suture, located west of the northern KS (Fig. 1c; Denkler et al., 1993, 1994; Harms et al., 1994; Schandelmeier et al., 1994; Stern et al., 1994).

(ii)   Then, an oblique convergence resulted into arc-continent collision and the final closure of the oceanic reentrants and the Mozambique oceanic basin between the ANS-related terranes and the Saharan meta-craton, leading to Atmur-Delgo and Keraf suturing between *ca.* 750-640 Ma (Abdelsalam et al., 1998).

(iii)   Finally, oblique convergence was translated into sinistral shearing along the KS which led to its superimposition by the KSZ at *ca.* 640-580 Ma (Abdelsalam et al., 1998).

6

The late to post-collisional lateral displacement occurred between *ca.* 630-590 Ma and is mostly recognized along the southern part of the KSZ (Evuk et al., 2014).

(iv) The orogenic activity ended along the KS-KSZ at ~565 Ma (Bailo et al., 2003) and a post-orogenic gravitational collapse locally reactivated structures at ~550 Ma (Stern, 1994; Abdelsalam et al., 1995, 2003; Abdelsalam and Stern, 1996a, 1996b; Ahmed Suliman, 2000).

In the westernmost ANS, six deformation phases have been interpreted from satellite imagery by Abdelsalam et al. (1995). The first two ($D_{1/2ADS}$) relate to Atmur-Delgo suturing and their field expression is limited to the northwestern KS (Fig. 1c; Schandelmeier et al., 1994; Abdelsalam et al., 1995, 1998, 2003; Perret et al., 2020). They are not considered further as not identified in our study area. Field data more or less robustly confirmed the existence of the four last D_{1-AS} to D_{4-AS} deformation events, that are attributed to the formation of KS-KSZ (Fig. 1c; Ahmed Suliman, 2000). Details about the related structures and previous tectonic interpretations are provided in Table 1. However, one can doubt that up to six deformation phases can be robustly resolved at first by remote sensing in such a complexly deformed area. This is the reason why we decided not to match the D_{1-AS} to D_{4-AS} deformation history and rather propose our own structural interpretation below.
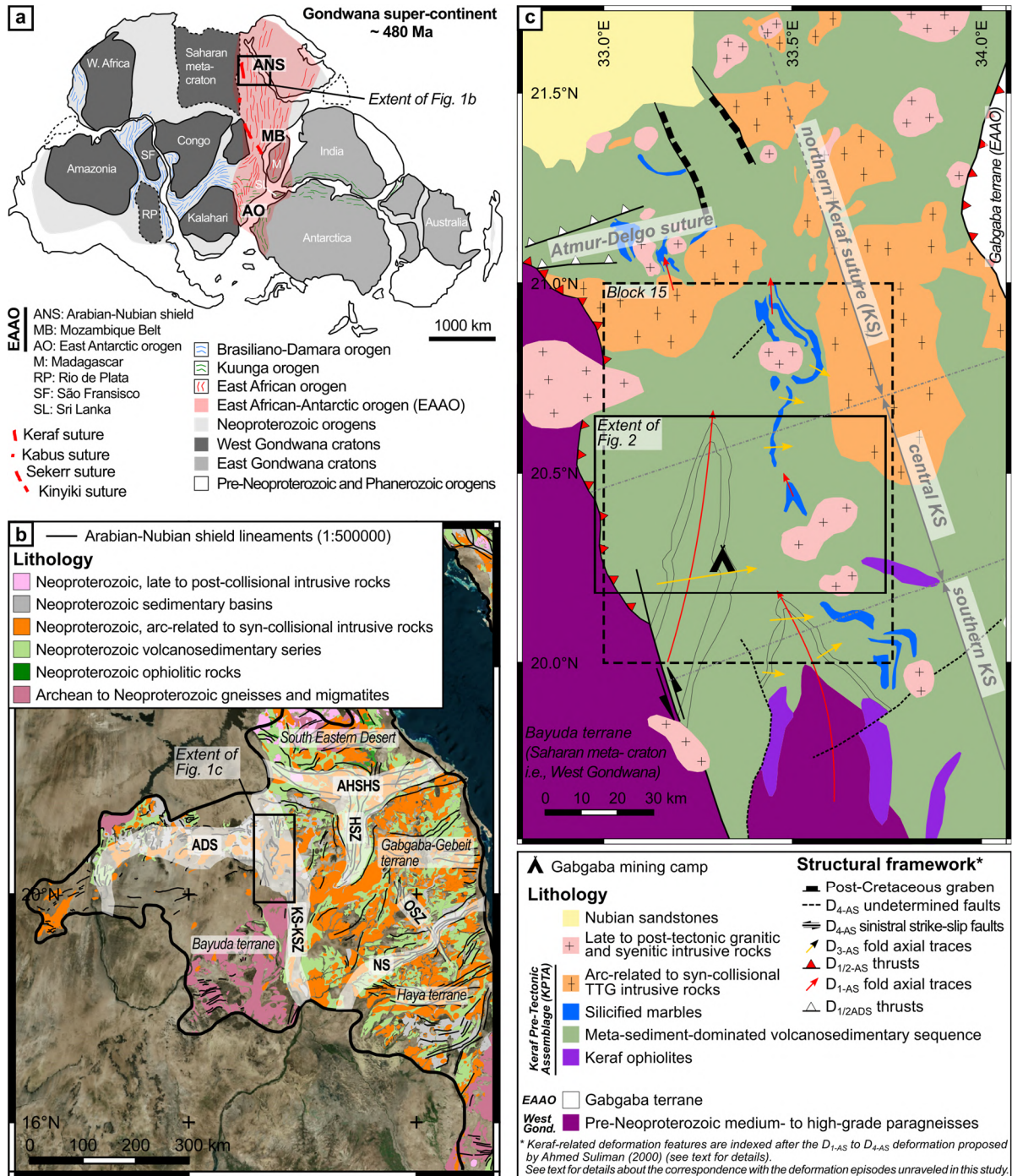
Figure 1: The Keraf suture in the framework of the East African-Antarctic orogeny (EAAO). **a** Gondwana super-continent reconstruction, modified after Gray et al. (2008). The location of the Keraf-Kabus-Sekerr-Kinyiki suture along the EAAO comes from Fritz et al. (2013). **b** Geological map of the Nubian part of the Arabian-Nubian shield (ANS).Lithological units are drawn from Egypt, Sudan and Eritrea national geological maps (Egyptian Geological Survey and Mining Authority, 1981; Geological Research Authority of the Sudan, 1988; Tadesse et al., 2000) after legend homogenization. The main suture and shear zones as well as terrane names are indicated after Johnson et al. (2011). Abbreviations are ADS = Atmur-Delgo suture; KS-KSZ = Keraf suture-shear zone; AHSHS = Allaqi-Heiani Sol Hamed suture; HSZ = Hamisana shear zone; NS = Nakasib suture; OSZ = Oko shear zone. Background is Google Satellite imagery from which lineaments have been drawn at 1:500000 scale. The extent of Figure 1c is indicated. Geographic coordinates are reported as WGS 84. **c** Geological map of the central Keraf suture (KS), from Ahmed Suliman (2000) and Bailo et al. (2003). The northern, central and southern KS limits are provided. "KPTA" stands for the Keraf Pre-Tectonic Assemblage described by Ahmed Suliman (2000) gathering all lithologies within the KS. The Block 15 exploration license hosts the Gabgaba gold district which this study focuses on. The extent of Figure 2 is indicated. Geographic coordinates are reported as WGS 84.

D_x	D_x-related structures	Deformation events (Ahmed Suliman, 2000)*
D_2 (**< 580 Ma**) **Minor gold event?**	**Any consistent significance at regional scale?** Rare north-striking east-dipping brittle F_2 fault planes reactivating C_{1b} shear zones. L_2 slickenlines plunging along the dip direction and stepped slip planes indicating top east-to-the-east normal-slip kinematics.	*None.* It is however worth noticing that north-striking normal faults are visible in the northeasternmost Saharan meta-craton, resulting from the tectonic collapse at the very end of the convergence between the ANS and the Saharan meta-craton (Denkler et al., 1994; Harms et al., 1994; Abdelsalam et al., 2003).
D_{1b} (***ca.* 640-580 Ma**) **Major gold event**	**Northwest-orientated oblique convergence, Keraf strike-slip shearing** Ductile-brittle coaxial-dominated general shear accommodating weak, non-coaxial, sinistral lateral displacement. From discrete, m-scale, brittle C_{1b} strike-slip faults to several km-scale C_{1b} shear zones and emplacement of a subvertical C_{1b}/S_{1b} penetrative shear band cleavage. Evidence for a dominant sinistral (block west-to-the-south) strike-slip shearing.	*D_{4-AS}:* brittle, northwest-orientated, sinistral Keraf transpression resulting from the translation of the northwest-orientated oblique collision between the future ANS and the Saharan meta-craton. Presence of conjugate sinistral northwest- and dextral northeast-striking strike-slip faults affecting all previous structures. **D_{4-AS} dominates the structural setting of the southern KS.**
	No corresponding structure observed in our study.	*D_{3-AS}:* roughly east-trending, symmetric, open folds superimposed over inherited fold patterns and are mostly visible from satellite imagery (Abdelsalam et al., 1995).
D_{1a} (***ca.* 700-640 Ma**)	**Northwest-orientated oblique convergence, Keraf suturing** Main ductile deformation stage controlling the regional structural framework. Formation of a roughly north-striking gently east-dipping S_{1a} penetrative cleavage and gneissic foliation affecting pre- to syn-tectonic meta-volcanosediments and intrusive bodies, respectively. The lithological contacts of these units also tends to get parallel to S_{1a} planes.	*D_{2-AS}:* ongoing Keraf suturing expressed by outcrop to regional-scale north-striking west-verging axial plane folds affecting the main penetrative cleavage in low-grade meta-sediments and ophiolites, fold interference and crenulation. *D_{1-AS}:* ductile deformation controlling the northern KS regional structural framework related to west-verging thrusting of the ANS upon the Saharan meta-craton. The main related structures are thrusts and folds visible at any scale and more or less affected by subsequent folding and strike-slip shearing at variable scales.

Table 1 *(continued)*

D_x	D_x-related structures	Deformation events (Ahmed Suliman, 2000)*
D_{1a} (*ca.* 700-640 Ma)	Rare evidence for a southeast-gently plunging L_{1a} stretching lineation along S_{1a} planes (kinematics?).	The related penetrative axial plane cleavage is the main planar fabric observed throughout the area and transposes the primary bedding in meta-sediments. The gently east-dipping main penetrative cleavage is thought to result from axial plan cleavage development together with a north-striking axial plane folding episode with a subvertical fold axis. Such folds, despite their several km wavelength according to Ahmed Suliman (2000), have not been observed during this study. **$D_{1\text{-AS}}$ and $D_{2\text{-AS}}$ dominate the structural setting of the northern KS.**

* Deformation episodes in the literature are indexed from $D_{1\text{-AS}}$ to $D_{4\text{-AS}}$ instead of D_1 to D_4 from the original work by Ahmed Suliman (2000), to avoid confusion with deformation indexing in this study. Rough age bracketing for each deformation stage is provided and discussed in the text. Deformation stages that relate to gold mineralization are indicated. Dashed lines indicate that D_{1a} and D_{1b} deformation stages are part of a single, prolonged, progressive deformation event whereas plain line indicates that D_2 is an independent deformation episode.

Table 1: Summary of the D_{1a}-D_{1b} and D_2 deformation episodes unraveled across the central Keraf suture.

3. Lithologies, structures and gold mineralization of the central Keraf suture

The geological map of the investigated area is available in Figure 2a. Outcrops discussed in this section and illustrated by Figs. 4 to 8, 10 and 11 are located in Figure 2b. Their geographic coordinates and description are reported in Table 2. A west-southwest-trending cross-section (extent in Fig. 2a) has been constructed across the studied area and illustrates the relationships between lithology and the main structures (Fig. 3).

Outcrop ID	Easting (°)	Northing (°)	Description
#1	33.298957	20.282872	Meta-andesite
#2	33.407881	20.434828	Meta-ash to lapilli tuff
#3	33.342592	20.299510	Layered meta-sediments
#4	33.003234	20.381444	Marble ridge
#5	33.236408	20.313202	Meta-igneous rock
#6	33.112477	20.285337	Granitic pluton
#7	33.183825	20.323270	Granitic pluton with mafic xenoliths and mingling texture
#8	33.297473	20.295830	Meta-sediments
#9	33.302725	20.284508	Meta-andesite and meta-diorite
#10	33.417345	20.474591	Meta-sediments
#11	33.412464	20.467093	Meta-volcanosediments
#12	33.139907	20.358596	Meta-diorite
#13	33.095032	20.343142	Meta-diorite hosting mineralized *en échelon* quartz veins (WG03 deposit)
#14	33.292320	20.280512	Meta-sediments and mineralized quartz veins (UTM deposit)
#15	33.339023	20.304732	Granitoid-hosted mineralized quartz vein network (Central Zone deposit)
#16	33.292368	20.283458	Mineralized quartz veins and their proximal off-shoots (UTM deposit)
#17	33.236408	20.313202	Distal off-shoot of vertical mineralized veins (UTM deposit)

Table 2: Geographic coordinates reported as WGS 84 and brief description of the key outcrops discussed in the text.
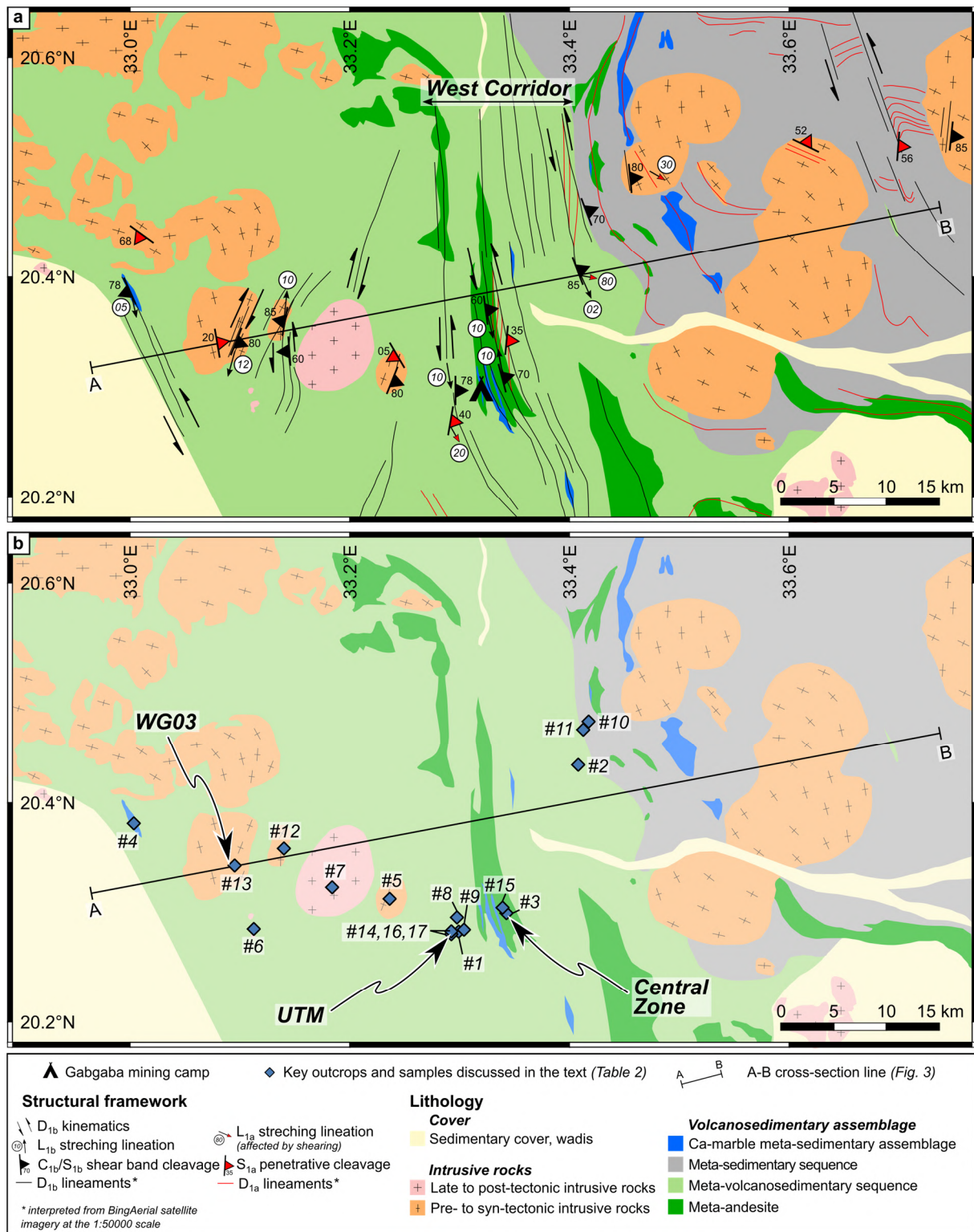
Figure 2: Geological map of the central Keraf suture hosting the Gabgaba gold district, adapted after Managem (2011) and relying on field observations. **a** Field structural observations and A-B cross-section line (Fig. 3). **b** Gabgaba gold deposits (UTM, WG03 and Central Zone) and locations of key outcrops and samples discussed in this study. Geographic coordinates are reported as WGS 84.
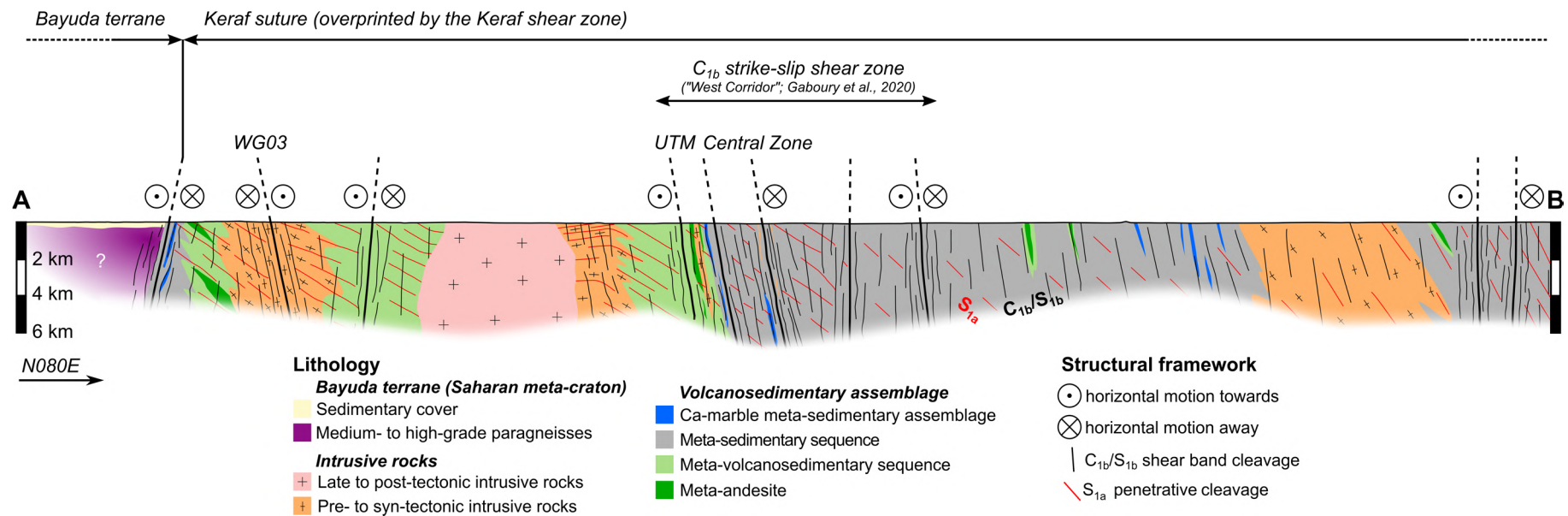
Figure 3: A-B crustal cross-section through the central Keraf suture. See Figure 2 for location.

3.1. *Lithological framework of the central Keraf suture*

The pre-, syn- and post-tectonic nature of lithologies observed in the central KS is relative to suturing tectonics. The pre- to syn-tectonic meta-volcanosedimentary assemblage is predominant (Figs. 1c, 2a) and is composed of:

(i)   A meta-volcanoclastic sequence characterized by low-grade schistose meta-andesite and ash to lapilli tuffs (Fig. 4a, b). Andesite crops out well and its contact with the volcanoclastics is gradual to sharp, parallel to the main penetrative fabric (Fig. 3).

(ii)   Meta-sediments which are mostly composed of schistose turbidites. The bedding is visible where silty layers alternate with silty to sandy layers and it is transposed (*i.e.*, its original orientation is completely or nearly completely rotated to the plane of the deformation affecting it) along the main penetrative fabric in most places (Figs. 3, 4c). Meta-sediments are interlayered with meta-volcanoclastic rocks and do not necessarily crop out well. The transition from one unit to another is gradual and difficult to map from regional to outcrop scales (Figs. 1c, 2a, 3). Meta-turbidites alternate with Ca-marble ridges that form outcrop- to regional-scale reliefs with sharp contacts parallel to the main penetrative cleavage (Figs. 1c, 2a, 3, 4d).

Pre- to syn-tectonic meta-diorite to tonalite-trondhjemite-granodiorite (TTG) intrusive bodies are enclosed within this extensive meta-volcanosedimentary sequence (Figs. 1c, 2a, 4e). Outcropping pre- to syn-tectonic intrusives are affected by a gneissic foliation that is representative of the regional penetrative fabric (Fig. 3). Their contacts with the surrounding meta-volcanosedimentary rocks are sharp but sheared along the regional penetrative fabric (Figs. 2a, 3, 4e). Post-tectonic coarse granitic intrusive bodies typically crop out as up to tens of m-high piles composed of up to 10 m-large boulders (Fig. 4f). These rocks show no anisotropy at macroscopic scale. Granite plutons display local heterogeneities with the presence of mafic xenoliths and micro-granular enclaves with feldspar pheno- or xenocrysts (inset in Fig. 4f). Their contacts with surrounding rocks are sharp and cut across every inherited fabric (Fig. 3).

Figure 4: Lithologies of the central Keraf suture. Outcrop locations and structural legend as in Figure 2. **a** Meta-andesite. **b** Meta-volcanoclastites. **c** Meta-sediments. **d** Ca-marble ridges. **e** Pre-tectonic intrusive rocks. **f** Post-tectonic intrusive bodies.

3.2.   Structural framework of the central Keraf suture

Three deformation stages and phases (D_{1a}, D_{1b} and D_2) have been defined. The *"stage" vs "phase"* nomenclature and indexing of deformation events relies on the distinction between progressive and discrete deformation (Fossen et al., 2019), which is discussed in subsection 4.1. The brittle *vs* ductile nature of the associated structures, which is a scale-sensitive description (Rutter, 1986; Snoke et al., 1998), is distinguished on field-scale observation. Similar to the approach followed by Perret et al. (2020), such nomenclature is used *"to distinguish the dominant manner by which deformation occurs"* (Tikoff et al., 2013): brittle deformation for faulting and fracturing and ductile deformation for penetrative fabric development and folding (Twiss and Moores, 2007). Table 1 summarizes D_{1a}-, D_{1b}- to D_2-related structures, as well as their correlation with the $D_{1\text{-AS}}$ to $D_{4\text{-AS}}$ tectonic history from literature.

3.2.1. Ductile D_{1a} deformation stage

A rare S_0 bedding is observed in meta-turbidites, highlighted by compositional layering between coarser-grained meta-greywackes alternating with finer-grained phyllitic beds (Figs. 4c, 5a and b). Considering rare outcrops, S_0 is the dominant planar fabric although it can be weakly to moderately crenulated along the northwest-striking S_{1a} crenulation cleavage (Fig. 5a, b).

At the studied area scale, the S_{1a} fabric is the dominant planar fabric and affects every pre- to syn-tectonic lithological units (Fig. 2a). In most places where meta-sediments crop out, the S_0 bedding is hardly visible because its orientation rotates to get parallel, *i.e.,* transposed, to the S_{1a} crenulation cleavage, resulting in a $S_{0/1a}$ composite fabric (Figs. 4c, 5a and b). S_{1a} is also the gneissic foliation affecting igneous intrusive bodies and the penetrative cleavage affecting andesitic rocks (Figs. 2a, 4a, 6a and b) and volcanosediments (Figs. 2a, 6c and d). Where not affected by subsequent deformation, the S_{1a} penetrative fabric is north-northwest- to north-northeast-striking and gently dips

eastwards whereas it is subvertical and strikes north-northwestwards where rotated by later C_{1b} shear zones (Fig. 6e). A stretching lineation L_{1a} is hardly visible along S_{1a} planes and weakly highlighted by stretched clasts in meta-lapilli tuffs (Fig. 6d). Along planes not affected by subsequent deformation, L_{1a} gently plunges southeastwards whereas it steepens where S_{1a} orientation gets closer to subsequent C_{1b}/S_{1b} shear band cleavage (Fig. 6f). No shear sense indicator is visible.

### 3.2.2. Ductile-brittle D_{1b} strike-slip shearing stage

D_{1b} structures range from regional- to outcrop-scale ductile shear zones (Figs. 2a, 3, 6d, 7a, b, and c) to local, discrete brittle faults (Figs. 5c, d, e and f, 6c). Depending on the D_{1b} strain intensity and the deformed rock rheology, the C_{1b}/S_{1b} shear band cleavage (or C_{1b}-type shear band; Passchier and Trouw, 2005) penetrates only the less competent meta-sedimentary rocks. With increasing strain: (i) the regional penetrative fabric S_{1a} is preserved (Fig. 4c) and locally cut across by discrete, subvertical, weakly expressed C_{1b} strike-slip faults (Figs. 5c, d, e and f, 6c); (ii) ductile-brittle C_{1b}-type shear bands are characterized from outcrop to regional scales (Figs. 2a, 3, 4b, 6d); and (iii) S_{1b} locally becomes the main penetrative fabric in C_{1b} shear zones where there is a very low obliquity between S_{1b} and C_{1b} planes (Figs. 3, 7c and d). In the latter configuration, lithological contacts and the S_{1a} cleavage have rotated along C_{1b} planes (Figs. 2a, 3, 5d).

There is evidence for a very limited lateral displacement along C_{1b} shear zones which does not exceed a few centimeters at the outcrop scale, even in marbles which easily flow under low strain conditions yet (Figs. 2a, 4b, 5e and f, 7a). No discrete individual shear accommodating relatively important lateral offsets has been noticed neither, suggesting that C_{1b} shear zones are homogeneous. Nevertheless, C_{1b} shear zones likely accommodate a weak, non-coaxial, strike-slip component (Figs. 2a, 3) as suggested by (i) the relatively short left-lateral offset along C_{1b} strike-slip shears (Fig. 5c, d, e, f), (ii) C_{1b}-type shear band asymmetry (Figs. 2a, 6c), (iii) the subtle presence of subhorizontal stepped slip markers along C_{1b} planes (Figs. 6d, 7c), (iv) drag fold asymmetry in flowing marble layers
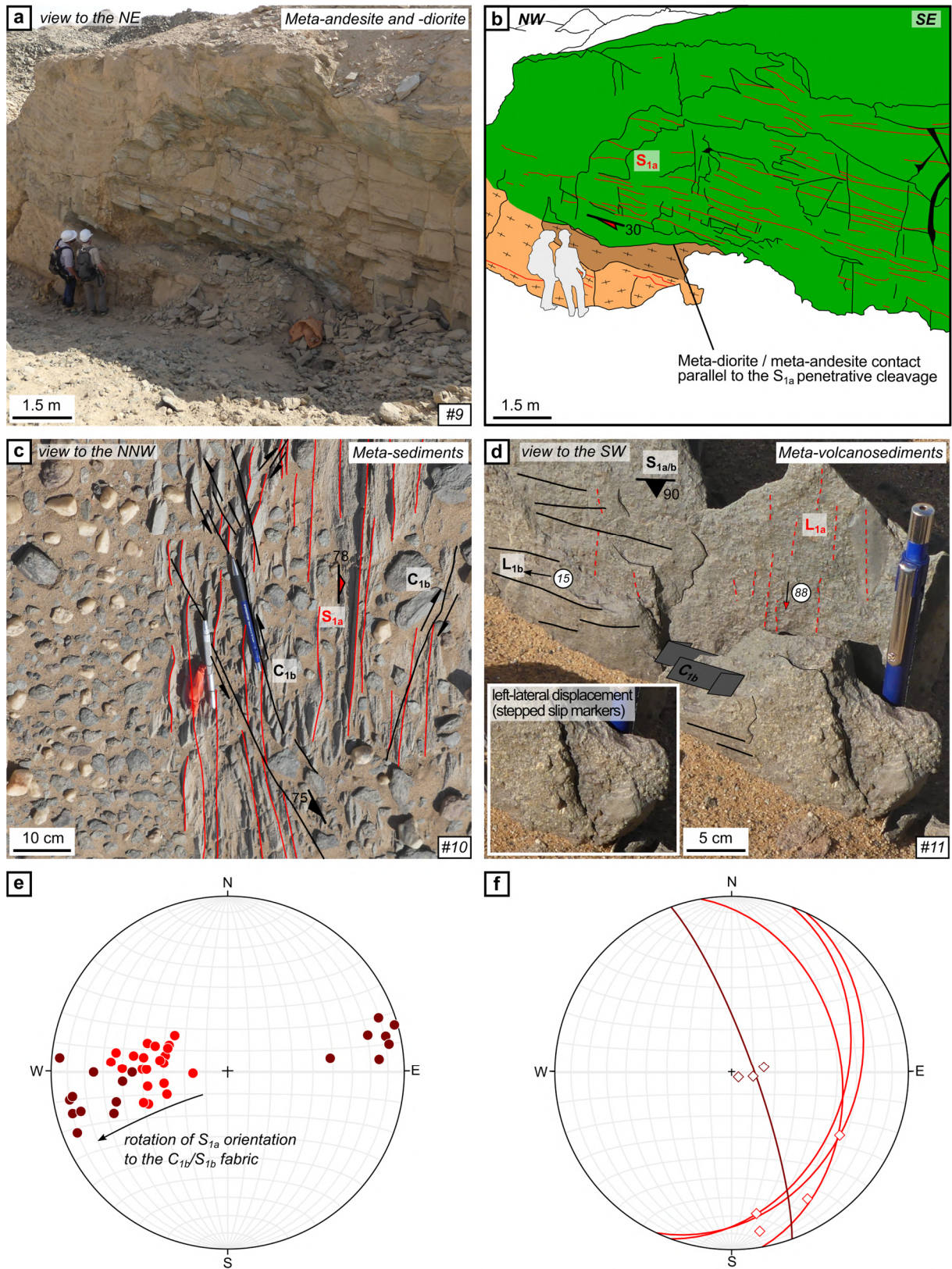
(Fig. 7a, b) and (v) the subhorizontal orientation of the L_{1b} stretching or biotite-amphibole mineral lineation along the C_{1b} planes (Figs. 2a, 7b, c and d). The C_{1b} shear zones are mostly subvertical and display two conjugate sets (Fig. 7e, f). The main C_{1b} strike-slip shears are north-northwest- to north-striking and accommodate sinistral strike-slip shearing (Figs. 2a, 3, 6c, 7d). North-northeast- to northeast-striking conjugate structures are less visible and display dextral kinematics (Figs. 2a, 3, 7e and f), relying on outcrop-scale shear sense indicators described above and deflection of D_{1a}-related lineaments visible in satellite imagery within C_{1b} shear zones (Fig. 2a).

3.2.3. Late brittle D_2 normal faulting phase

A late, weakly expressed, brittle D_2 deformation episode has been identified in the UTM area. It is characterized by the local reactivation of the C_{1b} shear zones as normal faults (Fig. 8). Shear zones reactivated as normal faults that have been spotted in this study preferentially separate rock units with a strong rheological contrast, *e.g.,* between meta-diorite or granitoid intrusion and meta-volcanosediments (Fig. 8a). F_2 faults are north-striking and steeply east-dipping, similarly to the C_{1b} shear zone orientation in the UTM area (Figs. 2, 8a). Weakly expressed L_2 slickenlines plunging along the dip direction and stepped slip features are visible on fault planes and indicate top-to-the-east normal faulting kinematics (Fig. 8b).
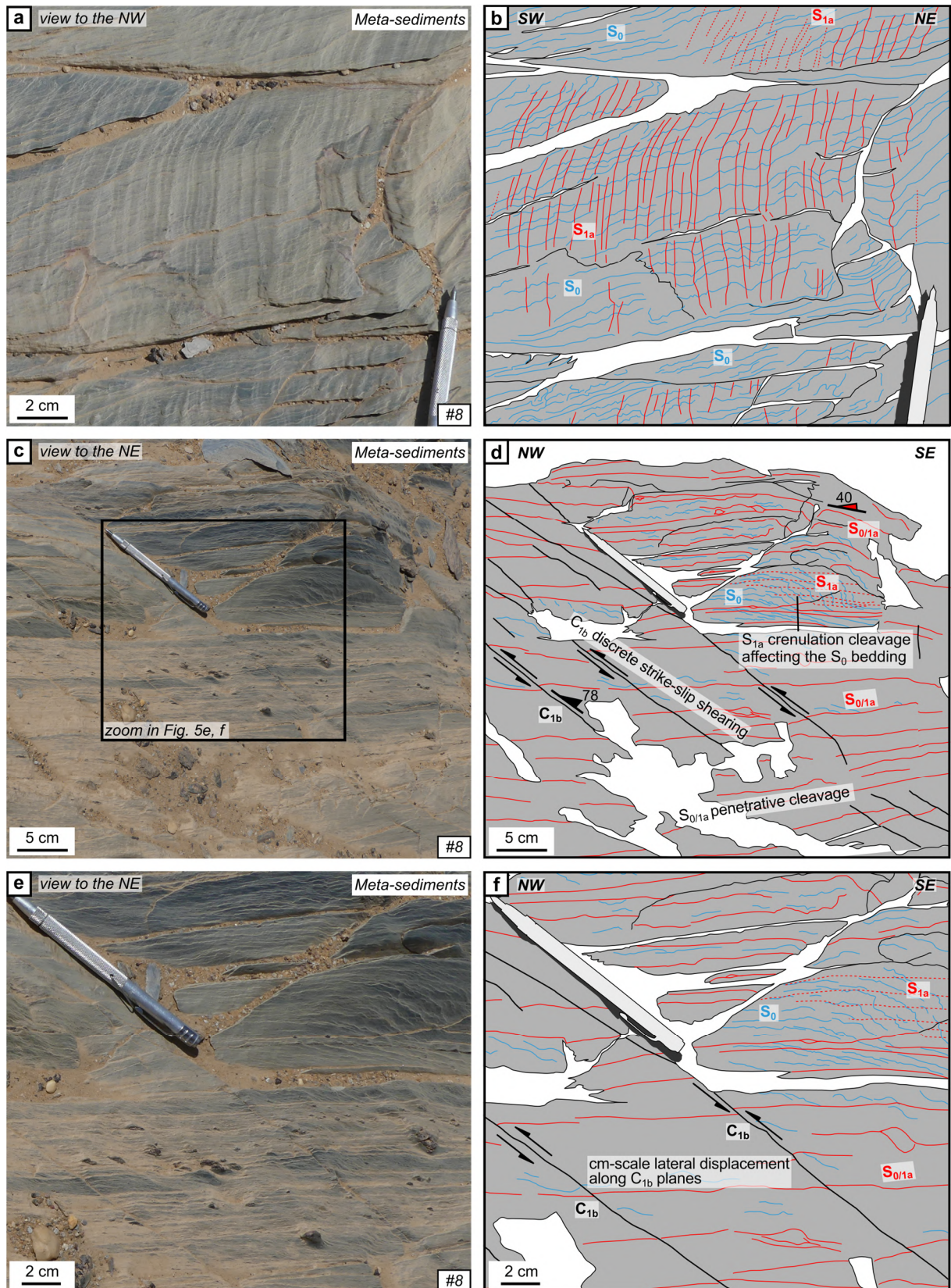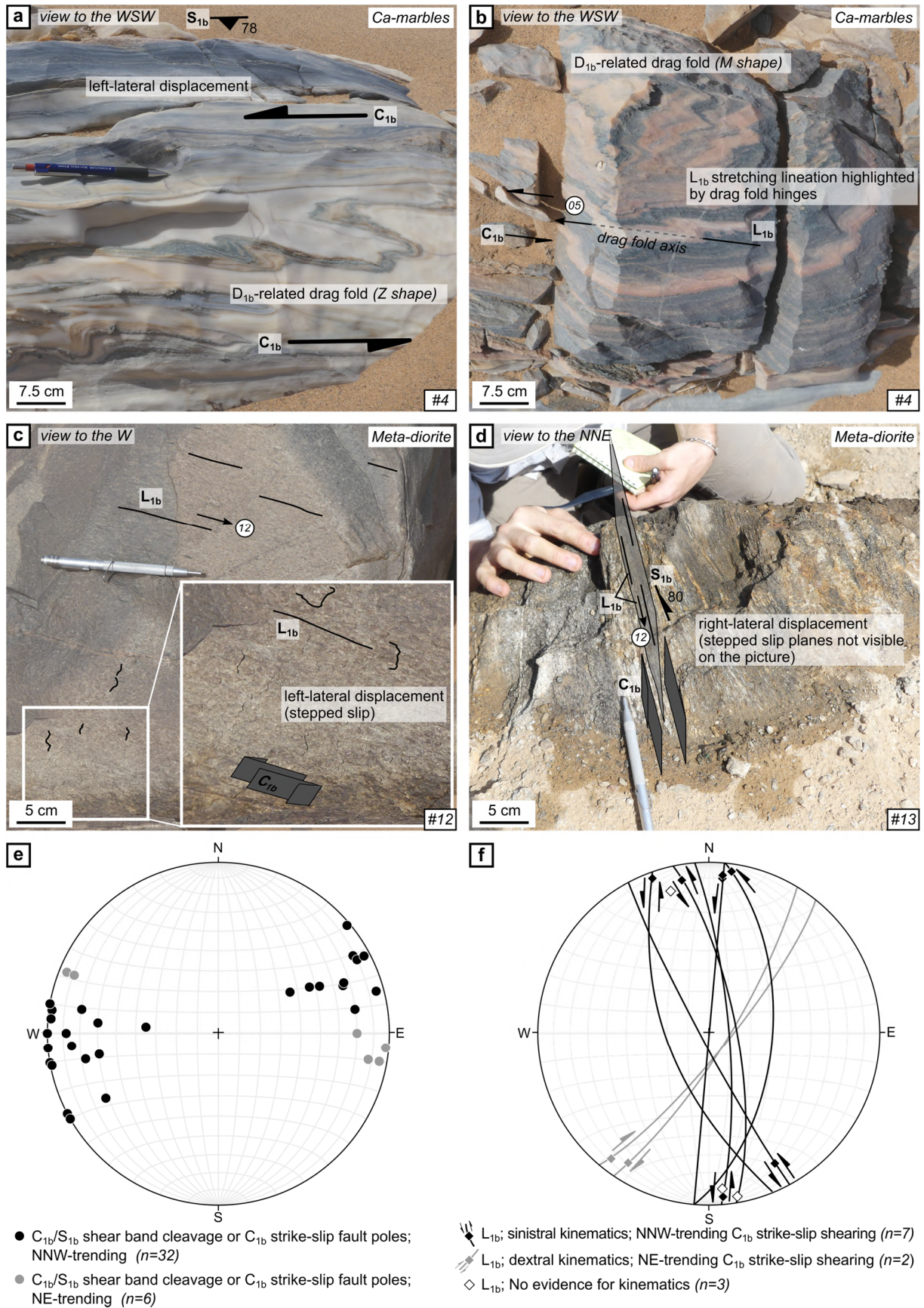
Figure 5: Outcrop expression of the S_0 bedding and relationships with the D_{1a}-D_{1b} deformation stages in meta-sediments. See detailed caption on p. 22.

Figure 6: Outcrop expression of the regional D_{1a} deformation stage in the Keraf pre-tectonic assemblage rocks, relationships with the D_{1b} deformation stage and stereonet analysis. See detailed caption on p. 22.

a *view to the WSW* S_{1b} ▼ 78   *Ca-marbles*

left-lateral displacement

C_{1b}

D_{1b}-related drag fold *(Z shape)*

C_{1b}

7.5 cm

#4

b *view to the WSW*   *Ca-marbles*

D_{1b}-related drag fold *(M shape)*

L_{1b} stretching lineation highlighted by drag fold hinges

05

C_{1b} *drag fold axis* L_{1b}

7.5 cm

#4

c *view to the W*   *Meta-diorite*

L_{1b} 12

L_{1b}

left-lateral displacement (stepped slip)

C_{1b}

5 cm

#12

d *view to the NNE*   *Meta-diorite*

S_{1b} 80

L_{1b}

12

right-lateral displacement (stepped slip planes not visible on the picture)

C_{1b}

5 cm

#13

e

N

W — E

S

f

N

W — E

S

● C_{1b}/S_{1b} shear band cleavage or C_{1b} strike-slip fault poles; NNW-trending *(n=32)*

● C_{1b}/S_{1b} shear band cleavage or C_{1b} strike-slip fault poles; NE-trending *(n=6)*

L_{1b}; sinistral kinematics; NNW-trending C_{1b} strike-slip shearing *(n=7)*

L_{1b}; dextral kinematics; NE-trending C_{1b} strike-slip shearing *(n=2)*

◇ L_{1b}; No evidence for kinematics *(n=3)*

Figure 7: Outcrop expression of the D_{1b} deformation stage in the Keraf pre-tectonic assemblage rocks and stereonet analysis. See detailed caption on p. 22.

Figure 5 (p. 19): Outcrop expression of the S_0 bedding and relationships with the D_{1a}-D_{1b} deformation stages in meta-sediments. Outcrop locations and geological legend as in Figure 2. **a** and **b** Outcrop photograph and interpretation. The S_0 bedding is the dominant fabric and is weakly to moderately crenulated along the S_{1a} crenulation cleavage. **c** and d Outcrop photograph and interpretation. The S_0 bedding is strongly rotated to transposed along S_{1a} crenulation planes, resulting into a $S_{0/1a}$ penetrative cleavage. This fabric is cut across by discrete, C_{1b} strike-slip faults displaying sinistral kinematics, although lateral displacement is almost invisible at this scale. Rarer north- to north-northeast-striking dextral C_{1b} strike-slip faults are also visible. **e** and **f** Outcrop photograph and interpretation, zoom of the central part of photograph c. This zoom better illustrates the < cm to cm-scale left-lateral displacement along north-northwest-striking C_{1b} strike-slip faults.

Figure 6 (p. 20): Outcrop expression of the regional D_{1a} deformation stage in the Keraf pre-tectonic assemblage rocks, relationships with the D_{1b} deformation stage and stereonet analysis. Outcrop locations and geological legend as in Figure 2. **a** and **b** Outcrop photograph and interpretation. The schistose meta-andesite and foliated meta-diorite are affected by the S_{1a} regional penetrative fabric. Their contact is also parallel to this gently east-dipping fabric. **c** The S_{1a} penetrative fabric is cut across by subvertical C_{1b}-type shear bands. The weak S_{1a} orientation deflection close to C_{1b} planes indicates a cm-long left-lateral displacement. **d** The L_{1a} stretching lineation is weakly highlighted by stretched clasts in steepened S_{1a} planes within a C_{1b} shear zone. The S_{1a} fabric is transposed along the C_{1b}/S_{1b} shear band cleavage. Subhorizontal L_{1b} slickenlines associated with sinistral C_{1b} strike-slip shearing are visible. **e** S_{1a} distribution in the central Keraf suture. **f** L_{1a} distribution in the central Keraf suture.

Figure 7 (p. 21): Outcrop expression of the D_{1b} deformation stage in the Keraf pre-tectonic assemblage rocks and stereonet analysis. Outcrop locations and structural legend as in Figure 2. **a** and **b** Marble ridges flow in a ductile way along the steeply east-northeast-dipping C_{1b}/S_{1b} shear band cleavage. Internal drag folds highlight sinistral kinematics for the C_{1b} strike-slip shearing but the lateral displacement is very low, i.e., <50 cm. **c** The presence of a subhorizontal L_{1b} stretching lineation and stepped slip markers in C_{1b} planes highlights a left-lateral displacement. **d** The main penetrative cleavage is S_{1b} which is here parallel to C_{1b} orientation. A subhorizontal L_{1b} stretching lineation and stepped slip markers in C_{1b} planes highlight a right-lateral displacement, not visible on the photograph. **e** S_{1b} and C_{1b} distribution in the central Keraf suture. **f** L_{1b} distribution in the central Keraf suture.
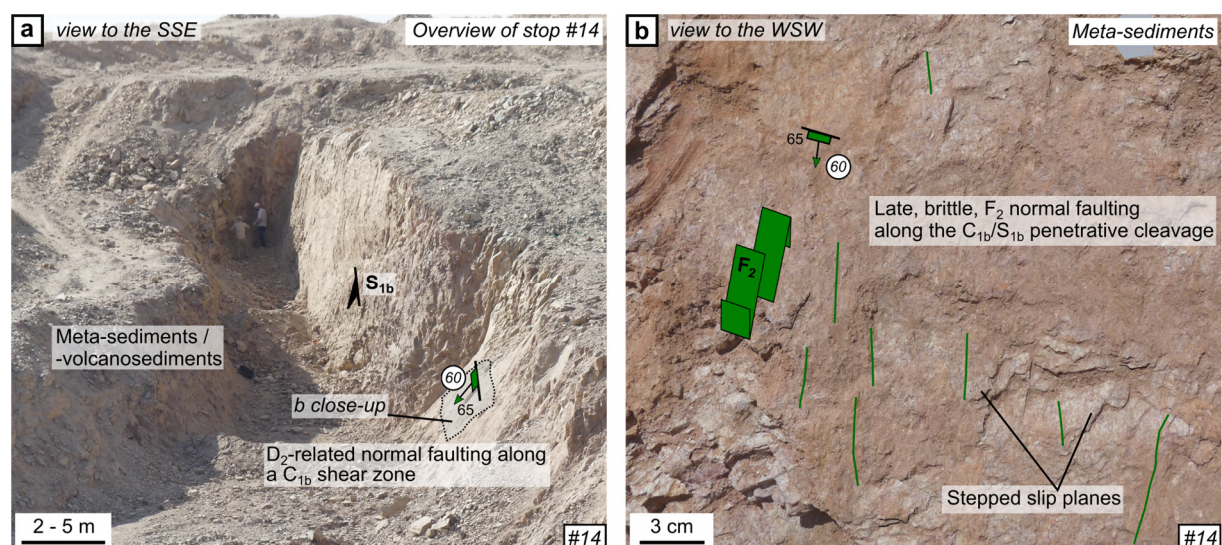
Figure 8: Outcrop expression of the D_2 deformation phase in meta-sediments. Outcrop location as in Figure 2. **a** Overview of the area investigated in Figure 8b. **b** C_{1b}/S_{1b} shear band cleavage is locally reactivated by brittle top-to-the-east F_2 normal faulting characterized by dip-plunging L_2 slickenline.

3.3.   *Mineralized structures of the Gabgaba gold district*

Deposit-scale geological maps of the WG03, Central Zone and UTM deposits are given in Figure 9a, b and c, respectively. Gold mineralized structures are illustrated from observations on outcrop, drill core and hand samples and thin section (Figs. 10 to 12, respectively). Stereonet structural analyses for the main gold-bearing structures at WG03 and Central Zone deposits are provided in Figure 13.
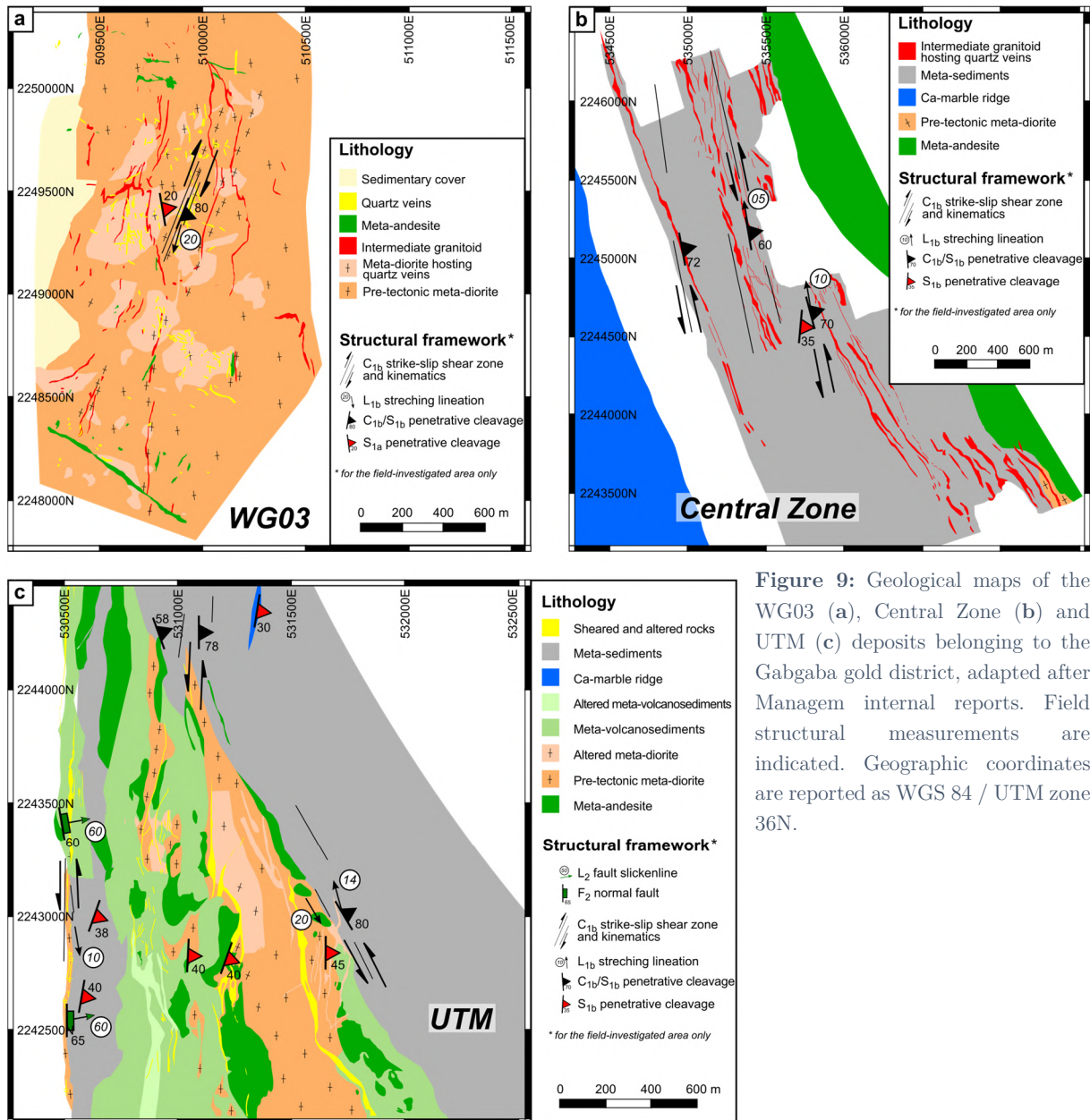

Figure 9: Geological maps of the WG03 (**a**), Central Zone (**b**) and UTM (**c**) deposits belonging to the Gabgaba gold district, adapted after Managem internal reports. Field structural measurements are indicated. Geographic coordinates are reported as WGS 84 / UTM zone 36N.

3.3.1. WG03 gold deposit

The WG03 deposit is located ~15 km west to the Gabgaba mining camp (Fig. 2b). It is hosted by a foliated pre-tectonic meta-diorite body affected by the north-northwest-striking gently east-dipping S_{1a} regional penetrative fabric (Figs. 9a, 10a). The meta-diorite intrusion is also cut across by numerous m-wide, northeast-striking, dextral C_{1b} shear zones (Figs. 9a, 10a) forming a km-wide shear zone at regional scale (Figs. 2a, 3, 10a). The host rock mineral assemblage mostly consists of amphibole, plagioclase and biotite, with minor quartz, titanite, magnetite and ilmenite (Figs. 11a, 12a and b).

Two gold mineralization events are observed at the WG03 gold deposit. The earliest mineralized features are not visible at outcrop scale. They consist of up to several cm-wide plagioclase-rich mineral assemblage segregated from the meta-diorite host rock (Fig. 11a). It is worth noticing that the use of the term "segregation" is used in a descriptive way below and does not imply anything about magmatic-anatexis petrological processes. The contact between these features and the gangue mineral assemblage is progressive and no sharp limit from one domain to another can be drawn at macroscopic and microscopic scales (Figs. 11a, 12a). The presence of these segregation features is associated with crystallization of plagioclase feldspar phenocrysts up to 10 cm away within the finer-grained amphibole-plagioclase-biotite mineral gangue (Fig. 11a, right). Pyrrhotite also forms at the transition between segregation features and host rock, associated with biotite and plagioclase (Fig. 12b). Where later gold-bearing structures are not visible, the presence of such plagioclase-rich patches correlates with gold grades ranging from 0.10 up to 1 g/t Au (Figs. 11a, 12a and b). However, no free gold grain nor micro-particle has been observed for such samples in thin section.

The subsequent gold-bearing structures are the most frequent at the WG03 deposit and characterized at outcrop scale. They are hydrothermal quartz-rich vein arrays cutting across the S_{1a} gneissic foliation and shaped like Type II *en échelon* veins (Fig. 10a, b; Bons et al., 2012). This hydrothermal vein set sharply cuts across the meta-diorite

gangue mineral assemblage and segregation features described above (Figs. 11b, 12c). Free gold grains are coeval with minor carbonation and moderate silicification spreading out from the vein margins (Fig. 12c, d). Gold grades range from <1 up to 30 g/t Au where the veins are observed, suggesting that the crosscutting quartz veining is the main gold mineralization event at the WG03 deposit (Figs. 11b, 12c and d). Despite the quartz internal crystal morphology is unclear in veins, the presence of coarse-grained quartz and the *en échelon* geometry of the vein array suggest that these veins are dilational (Figs. 10b, 11b, 12c). It means that they likely result from precipitation of minerals from fluids circulating in mode I-extensional fractures (Bons et al., 2012). The vein orientation progressively rotates from (i) subhorizontal to (ii) gently northeast-dipping and (iii) subvertical, north-northeast-striking with increasing deformation in lenses between C_{1b} shear zones, *i.e.,* veins progressively rotate parallel to C_{1b} planes and get transposed along them (Fig. 13a).

3.3.2. Central Zone gold deposit

The Central Zone deposit is located just east to the Gabgaba mining camp, within the several km-wide C_{1b} shear zone known as the *"West Corridor"* (Figs. 2a, 3, 9b). There, a subhorizontal stretching lineation L_{1b} plunges 10-12° northwards and shear sense indicators characterized the weak, left-lateral strike-slip component of the ductile-brittle shear zone (see above; Fig. 9b).

The gold mineralization corresponds to a well-developed vein system hosted by a network of granitoid intrusions in the Central Zone area (Fig. 9b). Shearing affects their contacts with surrounding meta-sediments (not illustrated in figures) but their inner part is not sheared and no penetrative fabric is visible at any scale (Figs. 10c, 11c and d, 12e). It is unclear whether these intrusions were injected along C_{1b} planes or are boudinaged and dismembered during D_{1b} deformation. The exact lithological nature of these granitoids remains unknown due to strong, pervasive sericitization-albitization spreading from vein margins (Fig. 12e). Yet, as the major element composition of the altered

granitoid is known (59 wt.% SiO_2, 19 wt.% Al_2O_3, 8 wt.% Fe_2O_3, 1 wt.% CaO, 5 wt.% Na_2O, 1 wt.% K_2O and 4 wt.% loss of ignition; unpublished data), we can approximate an intermediate to felsic nature for the unaltered protolith. The mineralized veins are a few cm up to 1 m-wide (Figs. 10c, 11c). Two sets of conjugate, connected veins are separated: the first ones are flat to gently west-northwest- or west-southwest-dipping whereas the second ones are gently east-northeast-dipping (Figs. 10c, 13b). They are composed of a quartz-ankerite-albite assemblage with a zoning from ankerite-albite-rich margins and quartz-rich core (Figs. 11c, 12e). Ankerite and albite crystals in vein display an elongate-blocky morphology perpendicular to vein walls and blocky quartz crystallization occurs as a final sealing stage (Figs. 11c right, 12e; Bons et al., 2012). It suggests that these syntaxial veins are purely dilational. Proximal pyritization of the host granitoids is associated with gold grades of about 0.1-1 g/t Au whereas up to 30 g/t Au concentration is reached where free gold is associated with quartz in veins (Figs. 11c and d, 12 e and f).

3.3.3. UTM gold deposit

The UTM deposit is located just west to the Gabgaba mining camp, within the *"West Corridor"* (Figs. 2a, 3, 9c). It is hosted by sheared and strongly chloritized meta-volcanosediments and foliated pre-tectonic meta-diorite intrusions (Fig. 9c). Granitoid intrusions similar to the ones described in the Central Zone area are visible along C_{1b} shear zones in the UTM area (Fig. 10d). There, late, F_2 normal faults reactivated C_{1b} shear zones along lithological-rheological contacts (Figs. 8a, 9c).

Gold-bearing quartz veins are currently being exploited at the UTM deposit. In the field, we were therefore able to approximate the gold potential of veins from how intensively they had been mined. The most important mineralized veins are subvertical, m-wide and formed along lithological-rheological contacts where F_2 normal faults are observed (Fig. 10d, e). These veins have never been characterized where C_{1b} shear zones occur with no evidence for late, normal faulting reactivation. However, the genetic

26

association between normal faulting and gold-mineralized veining remains uncertain as no kinematic evidence has been observed directly from the vein walls. Subvertical veins have off-shoots into the gently east-dipping S_{1a} cleavage affecting the surrounding meta-volcanosediments, outside from the F_2-reactivated C_{1b} shear zone (Fig. 10f). Off-shoots decrease in width down to a few cm at several tens of m away from the main gold-bearing, subvertical vein they spread from (Fig. 11e). At first sight, the mineral assemblage in mineralized veins and alteration halo at the UTM deposit is quite similar to what is observed for the Central Zone gold-bearing structures. UTM mineralized veins are quartz-ankerite-rich and somehow zoned with quartz-rich core and ankerite-rich margins (Fig. 11e). Veins are associated with proximal pervasive carbonation and pyritization of host rocks, whatever their lithology (Figs. 10e and f, 11e).

Unfortunately, we cannot go further with the observation of mineralization-deformation relationships at the UTM deposit. The area is indeed intensively exploited and only comprises very limited outcrops. Very few mineralized vein orientations have been measured and no reliable stereonet analysis is therefore possible. Besides, no observation on drill core and thin section has been made to better characterize relationships between macroscopic to microscopic gold-bearing structures, the related mineral assemblages and associated gold grades at the UTM deposit.
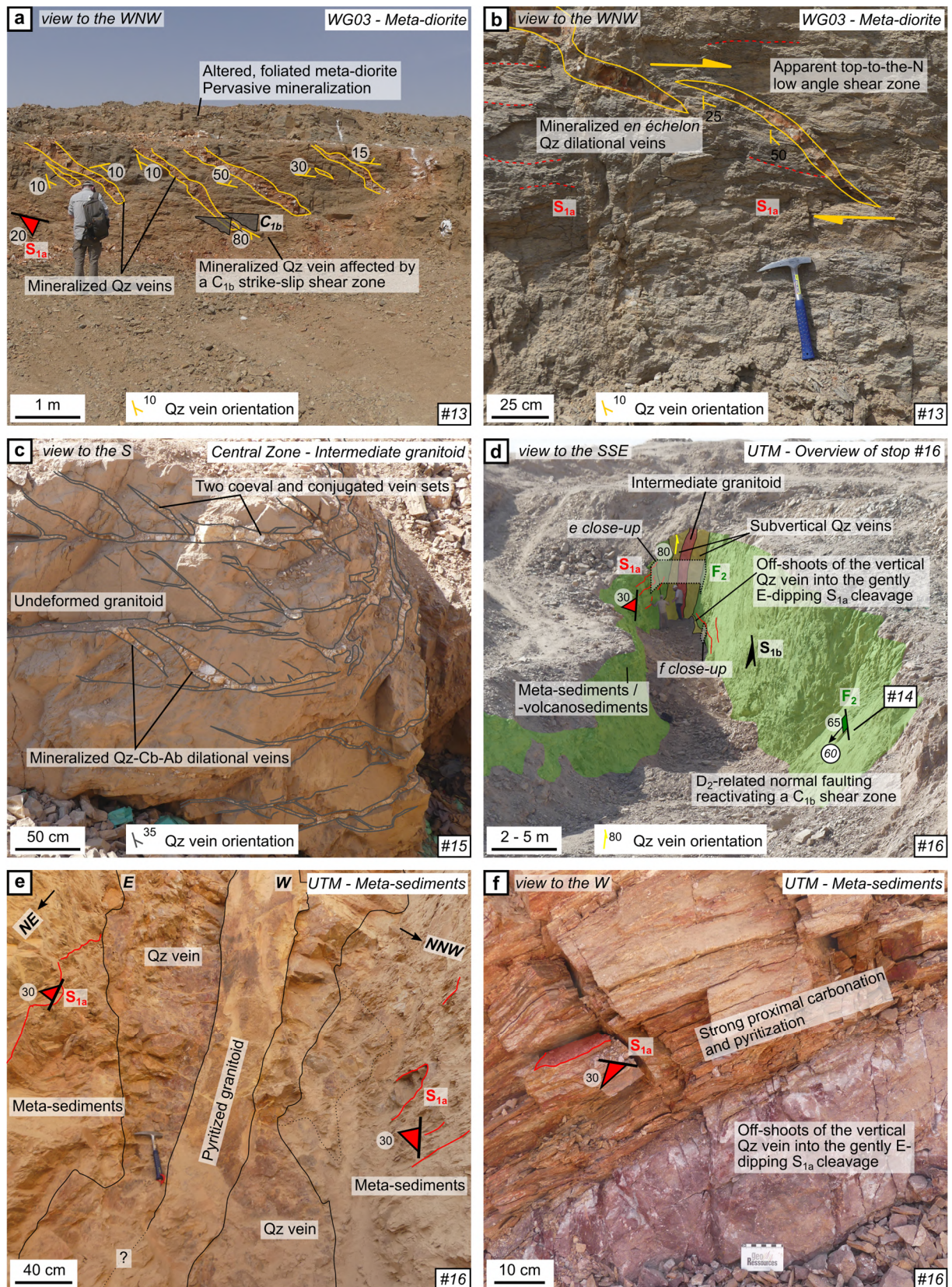
Figure 10: Gold-mineralized structures in outcrop at the Gabgaba gold district. See detailed caption on p. 31.
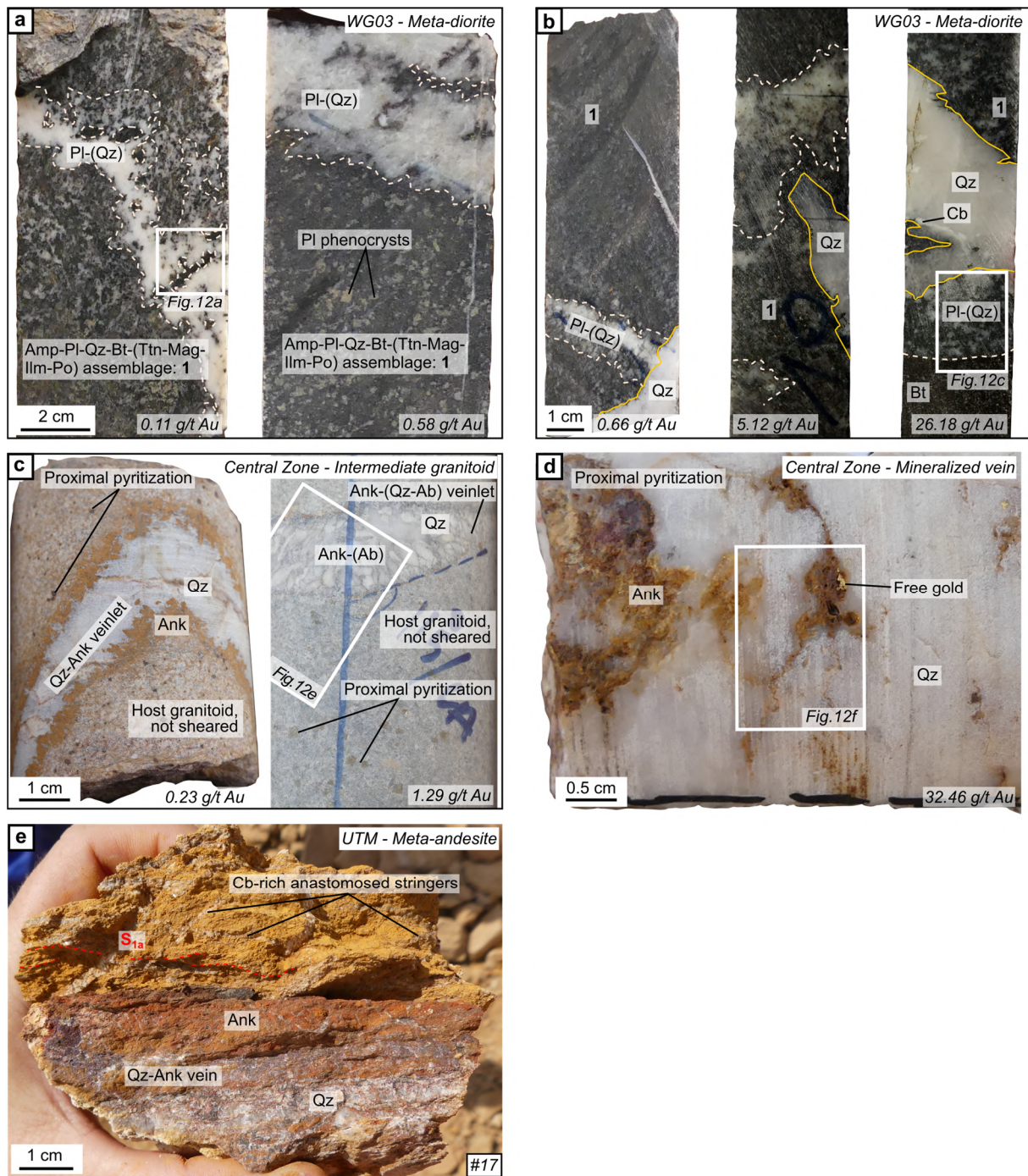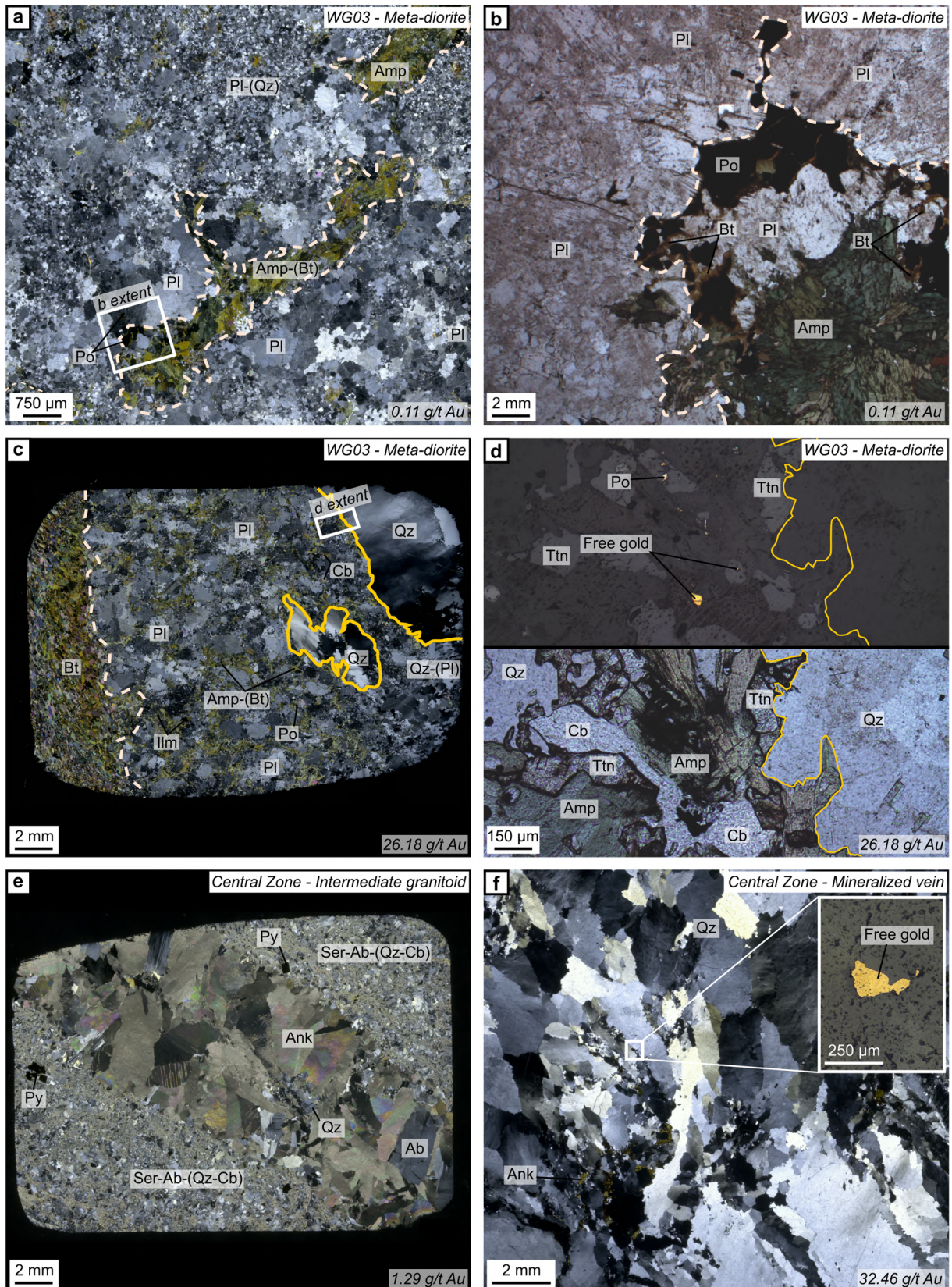
Figure 11: Gold-mineralized structures in drill cores and hand samples at the Gabgaba gold district. See detailed caption on p. 31.

Figure 12: Gold-mineralized structures at the microscopic scale at the WG03 and Central Zone gold deposits. See detailed caption on p. 31.

Figure 10 (p. 28): Gold-mineralized structures in outcrop at the Gabgaba gold district. Outcrop locations and structural legend are the same as in Figure 2 and mineral abbreviations are Ab = albite; Cb = carbonate; Qz = quartz. **WG03 deposit: a** Mineralized quartz vein arrays are formed within the pre- to syn-tectonic meta-diorite hosting the WG03 deposit and cut across the penetrative S_{1a} gneissic foliation. The S_{1a} fabric and veins are locally rotated along several m-scale C_{1b} strike-slip shear zones affecting the meta-diorite. **b** Where undeformed away from any C_{1b} strike-slip shear zone, the mineralized quartz veins are en échelon dilational veins. **Central Zone deposit: c** The Central Zone ore is characterized by conjugate quartz-ankerite-albite vein sets cutting across intermediate granitoids, with rare to no lateral extension within the surrounding meta-sediments. **UTM deposit: d** Overview of the area investigated in Figure 10e and f. An intermediate granitoid intrusion either formed or is deformed along a C_{1b} strike-slip shear zone affecting meta-volcanosediments. Later, the shear zone has been reactivated as a F_2 normal fault at the contact between the two rock units. The mineralization is hosted in veins along F_2 planes. **e** The main ore-bearing veins are subvertical. They form where the C_{1b} shear zone has been reactivated as a F_2 normal fault. **f** Subvertical ore veins have off-shoots into the gently east-dipping S_{1a} fabric, associated with a proximal carbonation and pyritization halo.

Figure 11 (p. 29): Gold-mineralized structures in drill cores and hand samples at the Gabgaba gold district. Outcrop locations are the same as in Figure 2b and mineral abbreviations are Ab = albite; Amp = amphibole; Ank = ankerite; Bt = biotite; Cb = carbonate; Ilm = ilmenite; Mag = magnetite; Pl = plagioclase; Po = pyrrhotite; Qz = quartz; Ttn = titanite. Gold grades for WG03 and Central Zone drill core samples are from Managem fire assay analysis database. **WG03 deposit: a** An early plagioclase-(quartz) segregation assemblage has fuzzy boundaries and no sharp limit with the meta-diorite mineral gangue, mostly composed of amphibole and plagioclase feldspar (simplified into "1" in Figure 11a and b). Plagioclase feldspar phenocrysts are locally visible up to a few centimeters away from the vein wall. The presence of such features in the bulk mineral assemblage is associated with relatively low gold grades between 0.10 and 1.0 g/t Au. The extent of Figure 12a is indicated. **b** Quartz-dominated mineralized veins with sharp contacts cut across the meta-diorite mineral gangue and early segregation features. Their presence is associated with low to higher gold grades (from <1.0 up to 30 g/t Au). The extent of Figure 12c is indicated. **Central Zone deposit: c** Gold-bearing quartz-ankerite-albite veins show a comb texture characterized by albite syntaxial growth perpendicular to vein wall. They are zoned with ankerite-albite crystallization at the vein margins and quartz at the core. A proximal pyritization is widespread through the host granitoid which is not sheared. The approximate extent of Figure 12e is indicated. **d** Where free gold is visible at macroscopic scale in dm-wide quartz-(ankerite) mineralized vein, gold grade can reach up to 30 g/t Au. The approximate extent of Figure 12f is indicated. **UTM deposit: e** Up to several tens of meters away from m-scale, subvertical mineralized veins (Fig. 10f), the width of quartz-ankerite-rich off-shoots into the S_{1a} fabric drastically decreases down to a few centimeters. These mineralized veinlets are zoned, with a quartz-rich core and ankerite-dominated margins. Anastomosed carbonate-rich stringers are formed in the proximal alteration halo associated with these veinlets.

Figure 12 (p. 30): Gold-mineralized structures at the microscopic scale at the WG03 and Central Zone gold deposits. Mineral abbreviations are Ab = albite; Amp = amphibole; Ank = ankerite; Bt = biotite; Cb = carbonate; Ilm = ilmenite; Pl = plagioclase; Po = pyrrhotite; Py = pyrite; Qz = quartz; Ttn = titanite; Ser = sericite. Gold grades for corresponding drill core samples are from Managem fire assay analysis database. **WG03 deposit: a** (cross-polarized, transmitted light) and **b** (plane-polarized, transmitted light) The transition from the amphibole-rich meta-diorite inclusion to the plagioclase-rich segregation zone is diffuse and there is no sharp contact between them where the bulk assemblage is mineralized. Pyrrhotite is associated with biotite in the contact area between these two domains. **c** (cross-polarized, transmitted light) and **d** (above: reflected light; below: plane-polarized, transmitted light) A quartz-dominated mineralized vein sharply cuts across the meta-diorite host rock and early plagioclase-rich features. Pervasive silicification spreads from the vein margins. Free gold mineralization is associated with pervasive silicification and carbonation. **Central Zone: e** (cross-polarized, transmitted light) and **f** (cross-polarized, transmitted light; inset: reflected light) A mineralized quartz-ankerite-albite vein sharply cuts across the ore-hosting granitoid intrusion strongly sericitized. Pyritization occurred at the vein selvages. Free gold grains are visible within quartz-dominated mineralized veins.

4. Interpretation of the tectonic and gold history of the central Keraf suture

4.1.   Tectonic evolution of the central Keraf suture

4.1.1. Progressive ductile to ductile-brittle D_{1a}-D_{1b} Keraf thrusting and strike-slip shearing

The ductile D_{1a} and ductile-brittle D_{1b} deformation stages control the structural setting of the central Keraf suture. Below, we interpret them regarding the formation of the KS-KSZ.

The ductile S_{1a} penetrative fabric gently dips eastwards between the C_{1b} strike-slip shear zones (Figs. 3, 6e). The rare observation of southeast-plunging L_{1a} lineation and absence of convincing passive markers that would allow assessing the amount and sense of displacement along S_{1a} planes suggest that D_{1a} deformation is coaxial-dominated general shear and that its non-coaxial component is weak. The regional penetrative fabric in the central KS is consistently attributed to Keraf suturing convergence in literature ($D_{1/2\text{-}AS}$ deformation in Fig. 1c and Table 1; Abdelsalam et al., 1998; Ahmed Suliman, 2000; Gaboury et al., 2020). At ANS scale, the significant stretching lineations are southeast-trending and were interpreted as associated with nappe emplacement with a tectonic transport from the southeast or the northwest (Shackleton et al., 1980; Ries et al., 1983; Sturchio et al., 1984; Shackleton, 1986; Bennett and Mosley, 1987; Greiling et al., 1988, 1994). We therefore propose that the ductile D_{1a} deformation stage expresses west- to northwest-verging thrusting during Keraf suturing, given the orientation of L_{1a} lineation in the studied area, despite the lack of kinematics evidence.

Ductile C_{1b} shear zones are subvertical and mostly strike north-northwestwards with left-lateral displacement, although rare north-northeast-striking, dextral shear zones have been observed (Figs. 2a, 3, 7f). These structures are attributed to the KSZ superimposition to the KS in literature, although they have previously been described as brittle structures ($D_{4\text{-}AS}$ deformation in Fig. 1c and Table 1; Abdelsalam et al., 1998;

Ahmed Suliman, 2000; Gaboury et al., 2020). We therefore suggest that D_{1b} deformation expresses the late convergent, Keraf sinistral shearing. The formation of rarer conjugate C_{1b} shear zones may therefore fit with a roughly west-orientated compression. Besides, D_{1b} deformation is thought to be coaxial-dominated general shear, similarly to what is suggested for the previous D_{1a} stage, as left-lateral displacement along C_{1b} shear planes does not exceed tens of cm at the outcrop scale. Despite a presumed change from Keraf thrusting to strike-slip shearing, the formation of the KS-KSZ likely relates to a coaxial-dominated D_{1a}-D_{1b} deformation history thus.

Ductile structures dominate for both D_{1a} and D_{1b} deformation stages and the orientation of the S_{1a} fabric progressively rotated along ductile C_{1b}-shear planes in shear lenses at every scale (Figs. 2a, 3 and 6e). There is therefore no field evidence for a temporal break in convergence between the penetrative D_{1a} deformation stage and the formation of C_{1b} shear zones. Despite there is a change in the expression of the deformation style from thrusting into lateral strike-slip, this may be irrelevant to mention as the magnitude of the non-coaxial component remains unknown for D_{1a} and is thought to be weak for D_{1b}. Besides, there is apparently no drastic change in stress field from D_{1a} to D_{1b} deformation, both being consistent with roughly west- to northwest-orientated compression. We therefore consider that the D_{1a} to D_{1b} deformation stages form a single, progressive, ductile to ductile-brittle deformation episode in a compressional regime (Fossen et al., 2019). Further stress field analysis and geochronological data would be required to confirm the latter hypothesis or prove otherwise.

4.1.2. Late, brittle, local D_2 extension regime and normal faulting

The tectonic history recorded in the central KS ends with a late, brittle, extensional D_2 deformation episode characterized by discrete, north-striking, east-dipping normal faults (Fig. 8). They have only been observed in the UTM area and their spatial extent is limited to less than a hundred meters (Fig. 9c). Normal faults reactivate C_{1b} shear zones, especially where rheological contrast is enhanced (*e.g.,* between intermediate

granitoid or meta-diorite intrusions and meta-volcanosediments). If these normal faults are certainly post-KSZ, their significance at regional scale is likely limited.

4.2. Gold mineralization events of the central Keraf suture

The mineralization-deformation relationships observed at the WG03, Central Zone and UTM deposits suggest that several mineralization events contributed to the overall gold endowment of the Gabgaba district. They are interpreted in terms of relative timing regarding the central KS tectonic evolution below.

4.2.1. Minor, low-grade, pre-D_{1a} gold event (WG03 deposit)

The first gold event characterized is limited to the WG03 deposit. It consists in plagioclase-rich segregation zones within the amphibole-dominated mineral gangue of the ore-hosting meta-diorite (Figs. 11a, 12a and b). There is no sharp boundary between these two domains and plagioclase feldspar is more or less abundant in both of them (Figs. 11a, 12a and b). These observations suggest that the segregation features may derive from magmatic-hydrothermal processes during the crystallization of the host meta-diorite rather than later hydrothermal processes. Similar textures were indeed observed for late magmatic *"pegmatitic veins"* at the magmatic-hydrothermal Cheechoo gold deposit, Canada (Fontaine et al., 2018; Turlin et al., 2019). However, additional work on fluid nature, composition of plagioclase feldspar and textural description must be carried out to better interpret the magmatic, magmatic-hydrothermal or hydrothermal nature of this mineralizing event. In this study, we only suggest that the first gold event recorded at the Gabgaba gold district is synchronous with pre-tectonic magmatism and therefore predates the regional D_{1a} deformation stage.

Gold grades associated with these segregation features range between 0.1-1 g/t Au and it has been checked in microscopy that gold mineralization is not related to subsequent micro-fractures bringing some gold later in the deformation history. The

absence of free gold associated with these features therefore suggests that gold is likely structurally bound in the lattice or occurs as nano-inclusions in other minerals, such as sulfides inclusions (*e.g.,* Cook and Chryssoulis, 1990; Reich et al., 2005; Hough et al., 2011; Deditius et al., 2014; Pokrovski et al., 2019; Combes et al., 2021). The only sulfide mineral observed is pyrrhotite which crystallizes at the transition between plagioclase- and amphibole-rich domains (Fig. 12a, b). Further analytical work such as LA-ICP-MS on sulfide should be carried out to test if invisible gold is trapped in pyrrhotite or not.

4.2.2. Major, high-grade, early to syn-D_{1b} gold event (WG03 and Central Zone deposits)

The main gold-bearing structures at the WG03 deposit are quartz-rich, *en échelon* veins crosscutting the S_{1a} gneissic foliation and associated with free gold mineralization and up to 30 g/t Au grades (Figs. 10a and b, 11b, 12d). The sigmoidal shape of the veins in cross section view, their probable dilational nature and the flat to gently north-dipping orientation of these veins in the least deformed parts of meta-diorite lenses between C_{1b} shear zones suggest that mineralized veins formed initially along top-to-the-north low angle shear zones (Figs. 10b, 12c, 13a, 14a). This interpretation relies on assuming that the vein opening is controlled by a north-orientated subhorizontal principal stress as indicated by the direction where *en échelon* vein tips point (Fig. 10b). However, there is no way to be certain that the vein geometry indicates the principal stress directions at the time when they formed as they must have been subsequently rotated at some extent in C_{1b} shear lenses. Where veins are more affected by D_{1b} strike-shearing, their orientation rotates counter-clockwise within the shear lenses, resulting in sigmoidal shapes in the horizontal plane (Figs. 13a, 14a). Veins are even transposed along north-northeast-striking subvertical C_{1b} shear veins where rotation has been the most intense (Figs. 13a, 14a). We therefore suggest that gold-bearing veining at WG03 postdates the D_{1a} stage and occurred early during the D_{1b} stage. The vein geometry model illustrated in Figure 14a could indeed fit with the presence of gently dipping extensional zones in an overall

strike-slip regime if an extensional jog between C_{1b} shear zones happens to be characterized. However, the C_{1b} shear zone traces are not well constrained at deposit-scale and step-over sites have not been recognized in the field (Fig. 9a). If further work is required to answer these questions, the main gold event at WG03 is likely part of the progressive deformation leading to the formation of the KSZ anyway.

Regarding the Central Zone deposit, given the granitoid array geometry and the fact that their contacts with surrounding meta-sediments are sheared, their intrusion likely predated their boudinage and dismembering along C_{1b} planes during the early D_{1b} deformation, *i.e.,* ductile formation of the KSZ, under a northwest-orientated compressional regime (Fig. 14b). Free gold-bearing veins (up to 30 g/t Au) preferentially cut across the granitoid intrusions because of their enhanced competency regarding the surrounding meta-sediments (Figs. 10c, 11c and d). The characterization of two sets of conjugate, connected, purely dilational veins which are flat to gently dipping eastwards or westwards indicates their formation occurred in a compressional regime. As the veins show no shear component, it is possible to reconstruct the finite main strain directions associated with their formation, provided that deformation is coaxial (Fig. 14b). The latter assumption is reliable as the D_{1a}-D_{1b} deformation controlling the structural setting of the central KS is interpreted to be coaxial-dominated general shear, despite a weak non-coaxial, strike-slip component must be considered for D_{1b}. In the proposed stereonet analysis, veining at Central Zone results from a south-southeast-orientated, subhorizontal shortening direction (Fig. 13b). It fits with the northwest-orientated compressional regime related to the KSZ strike-slip shearing: assuming that veins were formed in response to the latter compressional regime, they may look like the principal shortening direction is south-southeast-orientated due to clockwise rotation with sinistral shearing.

We therefore suggest that Central Zone gold-mineralized veining occurred during D_{1b} sinistral shearing and formation of the KSZ second-order *"West Corridor"* (Fig. 14b).
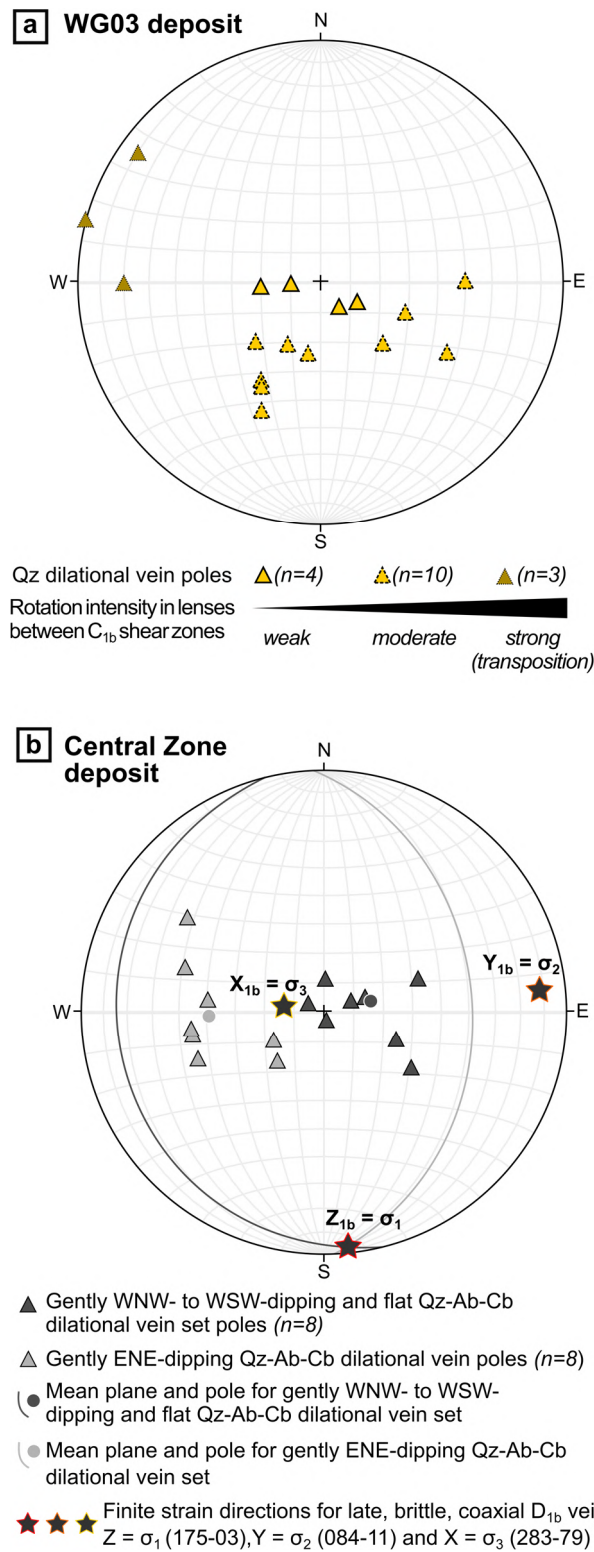
Figure 13: Stereonet analysis of the main gold-mineralized structures at the Gabgaba gold district. Mineral abbreviations are Ab = albite; Cb = carbonate; Qz = quartz. **a** Crosscutting quartz-dominated mineralized veins at the WG03 deposit. **b** Gold-bearing quartz-ankerite-albite veins hosted in granitoids at the Central Zone deposit.

37
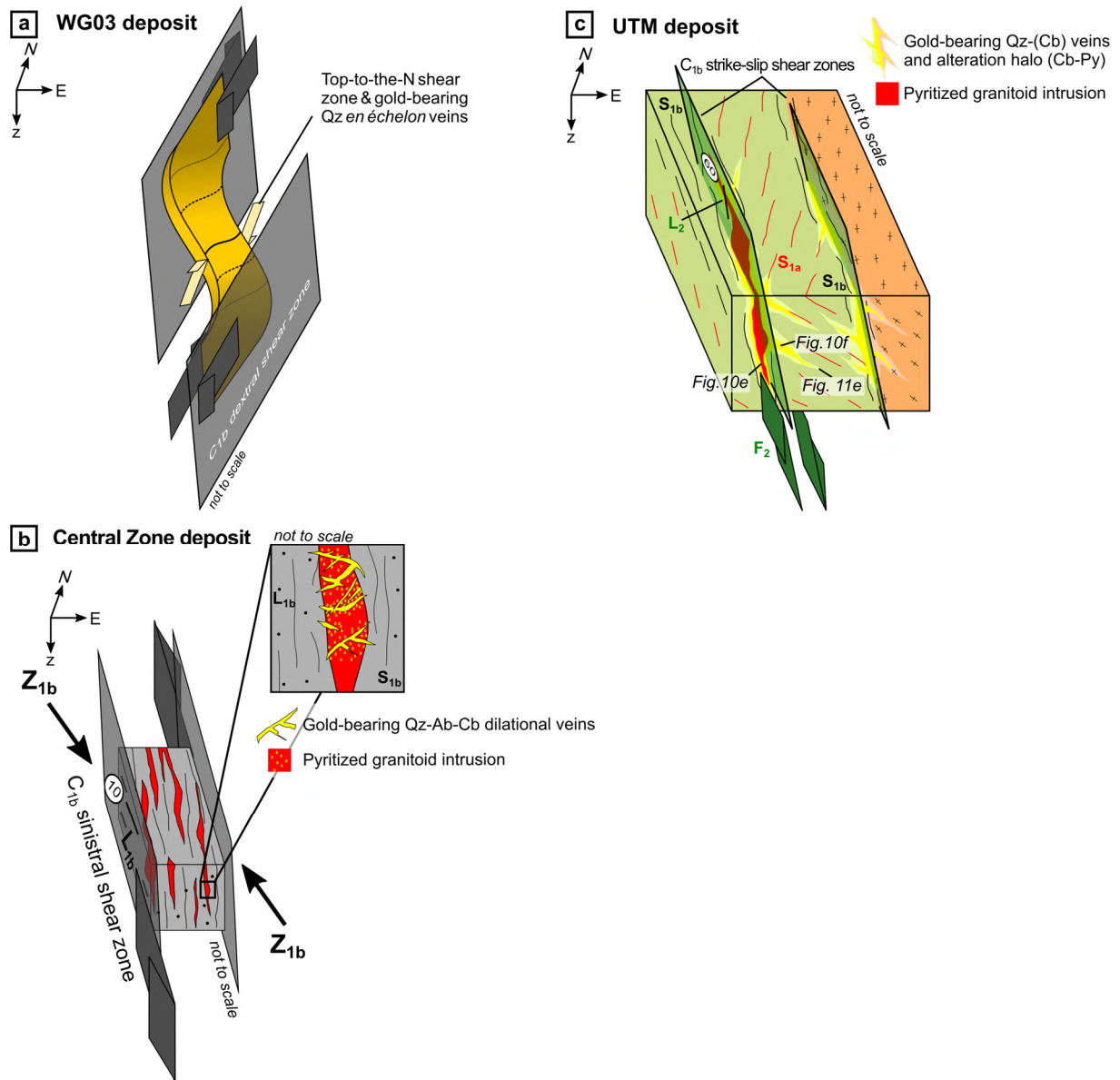
Figure 14: Tectonic interpretation for the formation of the main gold-bearing structures at WG03 (**a**), Central Zone (**b**) and UTM (**c**) deposits. The interpreted location of mineralized structures illustrated in Figs. 10e and f and 11e is indicated in **c**.

The WG03 and Central Zone deposits therefore highlight that a major gold event relates to progressive, ductile-brittle Keraf shearing in the central KS. According to gold grades, structure dimensions and density throughout deposit areas, the gold fertilization associated with this event is likely way higher than the gold budget represented by the early, pre-D_{1a} gold event defined at the WG03 deposit. However, we cannot conclude whether if D_{1a}-related gold results from (i) a new gold input in the system, (ii) the strong remobilization and local re-concentration of former gold, (iii) or a combination of both.

4.2.3. A late, syn-D_2 gold event (UTM deposit)?

Despite limited observations of deformation-mineralization relationships for the UTM deposit, we attempted to suggest a mineralization model for this deposit (Fig. 14c). The major gold-bearing veins currently exploited there are subvertical and formed along C_{1b} shear zones, only where they are reactivated as normal faults during the late brittle D_2 extensional deformation event characterized in the UTM area (Figs. 9c, 10d). The formation of these faults is favored where rheological contrast is strong, especially at contacts between rock units of variable competency, *e.g.,* granitoids and meta-sediments (Figs. 9c, 10d). We assume that fluid flow circulation and veining occurred along normal fault plane reactivation in an extensional regime. Besides, we propose that the inherited S_{1a} cleavage affecting surrounding meta-sediments is a very permeable fabric along which mineralizing fluid flow easily spread away from the fault. This mechanism would account for the presence of vein off-shoots and alteration halo into the S_{1a} fabric up to tens of m away from the main, subvertical veins (Figs. 10d and f, 11e, 14c). However, we lack key evidence to justify the genetic relationship between F_2 normal faults and subvertical veining as no normal-slip kinematic indicator is visible on vein walls. In addition, the very local extent and discrete manifestation of the D_2 deformation episode, limited to the UTM area, contrast with the strong gold endowment of the UTM deposit (see section 3).

Besides, it is worth noticing that the vein mineral assemblage dominated by quartz and carbonate, together with proximal pyritization, is quite similar to what is observed at the Central Zone deposit. Host lithologies are somehow the same as well, despite meta-diorite and schistose andesite are more abundant in the UTM area (Fig. 9b, c). We could thus legitimately wonder whether if these two deposits relate to the same mineralization event or not. We decided to separate them as the rheological control on mineralization is not expressed in the same way. At Central Zone, mineralized veins preferentially formed within granitoid intrusions deformed along C_{1b} shear zones whereas veins never

cut across the most competent plutonic units at UTM. Post-D_{1b} deformation should therefore be considered prior to or syn-veining at the UTM deposit to justify such a change in structural-rheological control on mineralization. Nevertheless, similarities between UTM and Central Zone deposits raise the possibility that the gold event characterized at the UTM deposit may overprint and/or result from remobilization of the major, syn-D_{1b} mineralized structures.

5. Discussion

Relying on our interpretation of the tectonic and gold history of the central Keraf suture (section 4), we now discuss similarities and differences with previous models and how the described deformation-mineralization events fit into the geodynamical evolution of the western Nubian shield.

5.1.   Reappraisal of the tectonic setting of the central Keraf suture

5.1.1. Towards a simplified and unified regional-scale tectonic history

Our study proposes that the central KS structural framework is dominated by progressive deformation with the succession of D_{1a} and D_{1b} stages, expressing the formation of the KS and KSZ, respectively, in a roughly west- to northwest-orientated compressional regime. Despite a change in plunge value, L_{1a} and L_{1b} lineations are mostly north-northwest- to northwest-striking (Figs. 6f, 7f). These lineations have already been identified in the ANS and Mozambique belt southwards (Abdelsalam and Stern, 1996b and references therein) and were further considered as indicating the direction of plate motion during Gondwana assembly (Shackleton and Ries, 1984). Our D_{1a}-D_{1b} model is therefore in agreement with previous studies suggesting that the formation of the KS and KSZ occurred in a prolonged, northwest-orientated, oblique convergence tectonic setting (Abdelsalam et al., 1995 , 1998; Ahmed Suliman, 2000). Rotation of the regional S_{1a} penetrative cleavage and early-D_{1b} ore *en échelon* veins of the WG03 deposit in shear

lenses between C_{1b} shear zones, whatever their scale, fits with this progressive deformation model. D_{1a} Keraf suturing is constrained between *ca.* 700-640 Ma (various age compilations; Stern, 1994; Abdelsalam and Stern, 1996b) and subsequent sinistral transpression is dated at *ca.* 640-580 Ma (lower age limit from Ar/Ar dating on hornblende and biotite in deformed granitoids (*e.g.,* Abdelsalam et al., 1995, 1998; Abdelsalam and Stern, 1996a, 1996b). We can therefore consider that the syn- to late convergence D_{1a}-D_{1b} deformation and formation of the KS-KSZ occurred between *ca.* 700-580 Ma (Table 1).

Later, brittle D_2 deformation is characterized by discrete, top-to-the-east normal faults in meta-volcanosediments, especially formed along rheological contacts within weakened C_{1b} shear zones. These normal faults have previously been observed in the Gabgaba gold district and interpreted as post-KSZ by Gaboury et al. (2020). However, very few orientation measurements have been made and these structures are very local in meta-volcanosediments. The regional significance of the extensional D_2 deformation episode therefore remains in abeyance. We can only consider that D_2 deformation occurred <580 Ma (Table 1). It is however worth noticing that significant north-striking normal faults have been characterized in the northeasternmost Saharan meta-craton, south to the Atmur-Delgo suture, a few hundred km away from the studied area. These extensional structures were attributed to a post-orogenic gravitational collapse that occurred ~550 Ma (Denkler et al., 1994; Harms et al., 1994; Abdelsalam et al., 2003).

Basically, the tectonic history unraveled within the central KS can be simplified into a single protracted deformation episode with a progressive change from thrusting to sinistral shearing, which is similar to the deformation episodes defined by Gaboury et al. (2020). Correspondence with deformation episodes of reference of the studied area, defined by remote sensing (Abdelsalam et al., 1995) and field work (Abdelsalam et al., 1998; Ahmed Suliman, 2000), is addressed in Table 1. The main S_{1a} penetrative fabric and sinistral C_{1b} strike-slip shear zones are well identified in both cases. However, most

of the complex structural interferences defined in literature, such as fold interference patterns associated with multiple regional- to outcrop-scale fold stages (Fig. 1c; Abdelsalam et al., 1995 , 1998; Ahmed Suliman, 2000), have not been characterized during this study. The regional-scale significance of these structures is therefore questionable.

5.1.2. Defining the central Keraf suture extent and deformation style

The Keraf suture is a poorly studied area with uncertain shape and boundaries (Gaboury et al., 2020 and references therein). For instance, Gaboury et al. (2020), in agreement with Abdelsalam et al. (1998), suggested that the central KS is relatively narrow. They consider that the western limit of the KS, *i.e.,* the contact between the Saharan meta-craton related Bayuda terrane to the west and the KPTA and Gabgaba terrane to the east (Fig. 1), is the several km-wide north-northwest-striking *"West Corridor"* hosting the Central Zone and UTM gold deposits (Figs. 2a, 3). If that was true, lithological units and deformation should be drastically different east and west of the *"West Corridor"*, expressing the transition from the Bayuda terrane westwards and the ANS eastwards. Yet, we observe the same lithological units and structures (S_{1a} and C_{1b}) east and west of the *"West Corridor"* (Figs. 2a, 3). Therefore, we would rather consider that the central KS is wider than suggested by Abdelsalam et al. (1998) and Gaboury et al. (2020), in line with the KS extent delimited by Ahmed Suliman (2000) (Figs. 1c, 2a, 3). The exact emplacement of the central KS western boundary could not be confirmed by field observations due to the presence of a Phanerozoic sedimentary cover overlying the Precambrian rocks of interest west of the limit from Ahmed Suliman (2000). The western extent of the central KS may thus remain underestimated.

Previously, the description of KSZ-related, second-order strike-slip structures was limited to the southern KS, where left-lateral displacement, if not estimated, is suggested to be more significant than for KSZ-related structures northwards (*e.g.,* Abu Dis and

Abu Hamed shear zones; Abdelsalam et al., 1998). However, although the structural framework of the central KS is dominated by Keraf suturing (D_{1a} deformation), C_{1b} shear zones are frequent within the central KS (Figs. 2a, 3). A C_{1b} shear zone notably overprints the interpreted Bayuda terrane-KPTA limit (Figs. 2a, 3). It contradicts Ahmed Suliman (2000) who suggested that this boundary was a D_{1a}-related thrust within the central KS (Fig. 1c). The central KS is therefore a complex area where the deformation style shifts between the thrusting- and strike-slip shearing-dominated northern and southern KS, respectively (Table 1; Abdelsalam and Stern, 1996b).

5.2. Polyphase gold dominated by syn-Keraf shear zone mineralization in the Gabgaba gold district

From field, macroscopic and microscopic observations, we suggest the existence of several gold events forming the Gabgaba gold district with distinct timing regarding the formation of the KS-KSZ (Fig. 15): (i) a first minor, pre-tectonic, (ii) a second major, late tectonic and (iii) a third potential, post-tectonic.

The first gold event we unraveled is low grade, *i.e.,* <1 g/t Au, and limited to the WG03 deposit. Disseminated pyrrhotite and the presence of feldspar-rich segregation-like features within meta-diorite characterize mineralization. Despite the magmatic or magmatic-hydrothermal nature of this ore event remains hypothetical at this point, we suggest it occurred with the pre-D_{1a} diorite intrusion (Fig. 15). We therefore suggest the existence of a first gold generation coeval with magmatic accretion, probably during oceanic subduction and Keraf arc-back-arc basin development, prior to ~750 Ma (Ries et al., 1985; Abdelsalam et al., 1998). Gaboury et al. (2020) did not distinguish this gold event at the WG03 deposit. Its contribution to the overall gold endowment is anyway thought to be very limited, regarding associated grades, dimensions and density of these mineralized features.

The major gold event forming most of the WG03 deposit and the entire Central Zone deposit broadly relates to *en échelon* ore veining as a response to the late collisional ductile-brittle D_{1b} shearing stage leading to the formation of the KSZ. The WG03 and Central Zone ore veins are associated with free gold mineralization and gold grades up to 30 g/t Au. Gaboury et al. (2020) observed the same major ore-bearing structures at Central Zone and WG03, with similar metamorphic, carbon-rich aqueous fluid signature for both deposits. They also attributed the mineralization event to the KSZ-related late oblique convergence, at the retrograde amphibolite-greenschist facies transition. The main difference is that Gaboury et al. (2020) attributed ore veining at Central Zone to reverse faulting at the contacts between granitoids and surrounding meta-sediments, rather than strike-slip shearing. These two options are however not mutually exclusive as (i) they both fit with a roughly northwest-orientated compressional regime and (ii) the non-coaxial component of D_{1b} deformation is thought to be very limited as discussed above. Besides, alteration is expressed by distal sericitization-(pyritization), proximal pyritization-carbonation and quartz-ankerite-albite-gold veining hosted in granitoids. The Central Zone deposit can therefore be considered as the perfect example for intrusion-hosted orogenic gold formed in a syn- to late compressional regime along second-order shear zones with typical structural, fluid, alteration and metamorphic footprints.

We attributed the formation of the UTM gold deposit to ore veining during late, brittle D_2 extension and normal faulting along reactivated shear zones. However, (i) the D_2 deformation is hardly interpretable as spatially limited to the UTM area, (ii) the genetic link between ore veins and normal faults is not clearly established and (iii) the UTM deposit displays numerous similarities with the Central Zone deposit. All these reasons make the interpretation of the UTM gold event highly uncertain. Vertical veins where not characterized by Gaboury et al. (2020) who only defined the gently east-dipping vein off-shoots into the regional S_{1a} fabric. They proposed that these veins formed

along reverse faults activated during the KSZ formation, within the second-order *"West Corridor"* hosting both the Central Zone and UTM deposits. Their interpretation is supported by a fluid signature in gold-bearing veins at UTM similar to the one reported at Central Zone and WG03. Besides, this option has the merit to simplify the gold history of the Gabgaba gold district, considering a single, syn-D_{1b} orogenic-like gold event accounting for most of the gold endowment in the central KS. The debate is still open.

Most of the gold mineralization in the central KS is therefore coeval with the late tectonic formation of the KSZ overprinting the KS. At Nubian shield-scale, ~600 My-old gold mineralization hosted by quartz veins and related to ductile-brittle transcurrent structures is mostly characterized as orogenic gold (*e.g.,* Elsamani et al., 2001; Klemm et al., 2001; Botros, 2002, 2004; Helmy et al., 2004; El Kazzaz, 2012; Osman, 2014; Helmy and Zoheir, 2015; Khalil et al., 2016; Fawzy, 2017; Zoheir et al., 2019a, 2019b, 2019c). However, there is also some evidence for gold mineralization during the magmatic accretion stage and early amalgamation of the ANS (*ca.* 830-640 Ma; age compilation by Abdelsalam and Stern, 1996b), such as the first gold event portrayed at the WG03 deposit or the syn-Atmur-Delgo suturing Galat Sufar South gold deposit (Perret et al., 2020). In the latter study, the authors indeed demonstrated that the regional Atmur-Delgo deformation shapes the local structural setting and controls the formation and geometry of ore-shoots from the deposit to the macroscopic scales. Even if less documented, the existence of pre- to early-suturing gold events across the ANS should therefore not be underestimated. To go further and better constraint the gold mineral system expressed along the central KS, it appears now critical to (i) track the regional lithospheric evolution, (ii) put geochronological constraints on the deformation and gold events and (iii) study their gold input or remobilization nature and the potential genetic links between these gold episodes.
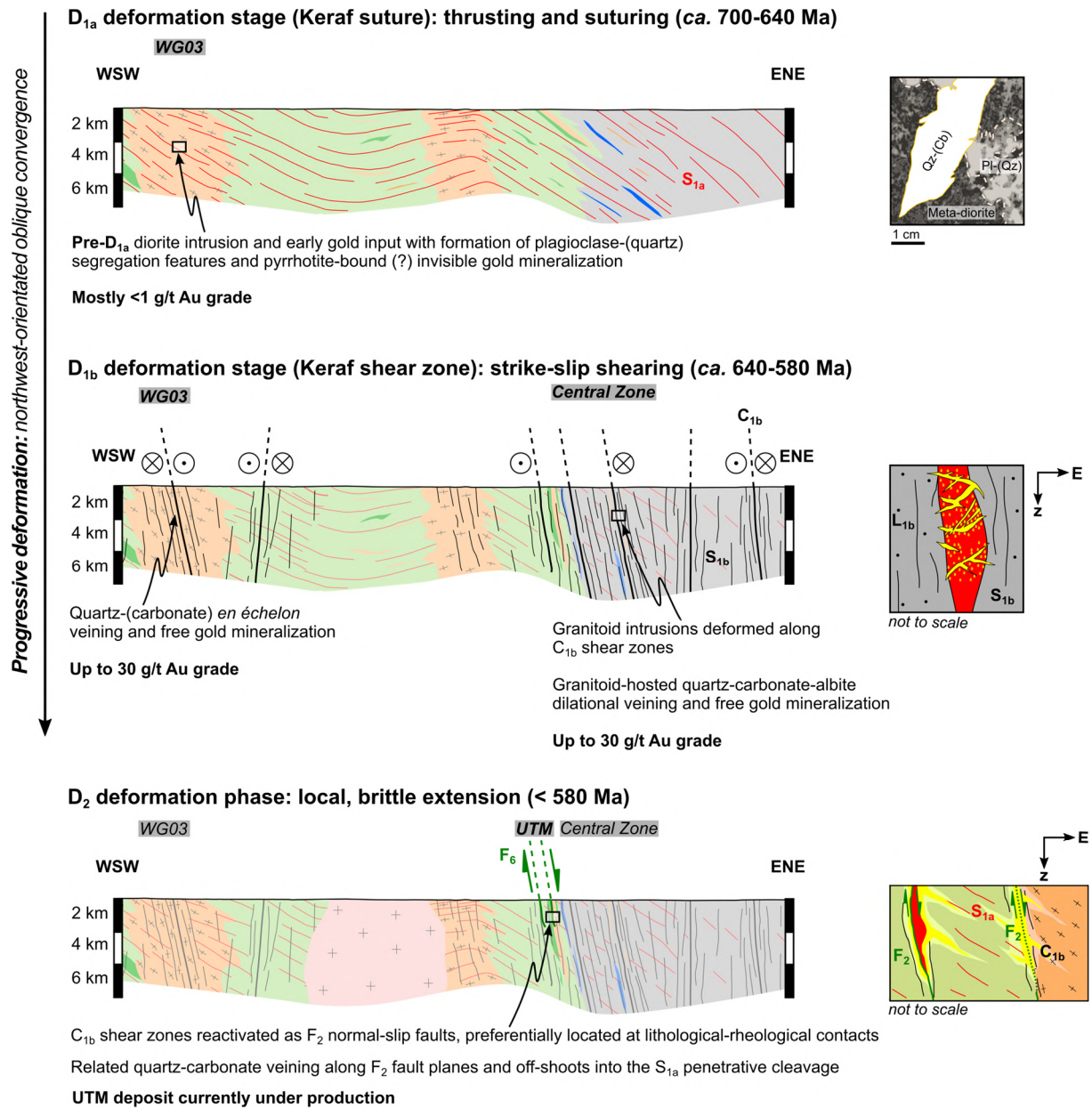
Figure 15: Relative timing of the Gabgaba district gold deposits (WG03, Central Zone and UTM) regarding the deformation history recorded by the central Keraf suture. Litho-structural legend is the same as in Figure 3 and mineral abbreviations are Cb = carbonate; Pl = plagioclase; Qz = quartz. See text for chronological constraint explanation and related references. Insets on the right correspond to schematic zooms of the black rectangle for each cross-section.

6. Conclusions

Field observations suggest that the structural framework of the central Keraf suture is dominated by a progressive, ductile to ductile-brittle D_{1a}-D_{1b} deformation characterized by the regional S_{1a} penetrative fabric and C_{1b} sinistral shear zones. This deformation relates to Keraf suturing and subsequent left-lateral shearing in a prolonged northwest-orientated compressional regime between *ca.* 700-580 Ma. However, the D_{1a}-D_{1b} deformation is thought to be coaxial-dominated shear and the non-coaxial deformation component, *i.e.,* vertical and lateral displacement along structure planes, is weak. A C_{1b} shear zone overprints the boundary between the central Keraf suture and the Saharan meta-craton westwards which was not documented by previous studies. The central Keraf suture can therefore be seen as a transition zone between the northern Keraf suture, dominated by D_{1a} deformation, and the southern Keraf suture where C_{1b} shear zones are more frequent. A late, brittle D_2 normal faulting event reactivated inherited C_{1b} shear zones. However, the significance of this deformation episode at regional scale remains uncertain as it is very local.

Relying on field and drill core relationships between structures and mineralization, we clearly define a polyphase gold history with two mineralizing events occurring in the ~30 km-wide Gabgaba gold district. The first one is pre-D_{1a} and related to magmatic accretion in the WG03 area but its contribution to the overall gold endowment is likely limited. The major gold event formed the WG03 and Central Zone deposits and is characterized by ore veining during late tectonic ductile-brittle Keraf strike-slip shearing. This mineralizing event can relate to orogenic gold, which is widespread at ANS-scale. The occurrence of a post-tectonic brittle gold event coeval with the D_2 deformation episode is suggested at the UTM deposit, but its existence remains highly uncertain.

Acknowledgements

References

Abdelrahman, E., Matheis, G., Schandelmeier, H., Karfis, M.A., Gadir, I.A., El Khedir, M., 2017. Evolution of the Keraf back-arc basin: Constraints on the Nubian Shield margin. Geoscientific Research in Northeast Africa. CRC Press, 93–98.

Abdelrahman, E.M.A., 1993. Geochemical and geotectonic controls of the metallogenic evolution of selected ophiolite complexes from the Sudan. Reimer.

Abdelsalam, M.G., Abdel-Rahman, E.-S.M., El-Faki, E.-F.M., Al-Hur, B., El-Bashier, F.-R.M., Stern, R.J., Thurmond, A.K., 2003. Neoproterozoic deformation in the northeastern part of the Saharan Metacraton, northern Sudan. Precambrian Research 123, 203–221. https://doi.org/10.1016/S0301-9268(03)00068-8

Abdelsalam, M.G., Dawoud, A.S., 1991. The Kabus ophiolitic melange, Sudan, and its bearing on the western boundary of the Nubian Shield. Journal of the Geological Society 148, 83–92. https://doi.org/10.1144/gsjgs.148.1.0083

Abdelsalam, M.G., Stern, R.J., 1996a. Mapping Precambrian structures in the Sahara Desert with SIR-C/X-SAR radar: The Neoproterozoic Keraf Suture, NE Sudan. Journal of Geophysical Research: Planets 101, 23063–23076. https://doi.org/10.1029/96JE01391

Abdelsalam, M.G., Stern, R.J., 1996b. Sutures and shear zones in the Arabian-Nubian Shield. Journal of African Earth Sciences 23, 289–310. https://doi.org/10.1016/S0899-5362(97)00003-1

Abdelsalam, M.G., Stern, R.J., Copeland, P., Elfaki, E.M., Elhur, B., Ibrahim, F.M., 1998. The Neoproterozoic Keraf Suture in Ne Sudan: Sinistral Transpression Along the Eastern Margin of West Gondwana. The Journal of Geology 106, 133–148. https://doi.org/10.1086/516012

Abdelsalam, M.G., Stern, R.J., Schandelmeier, H., Sultan, M., 1995. Deformational History of the Neoproterozoic Keraf Zone in NE Sudan, Revealed by Shuttle Imaging Radar. The Journal of Geology 103, 475–491. https://doi.org/10.1086/629771

Ahmed Suliman, E.T.B., 2000. KERAF SHEAR ZONE, NE SUDAN: GEODYNAMIC CHARACTERISTICS OF THE NILE CRATON-NUBIAN SHIELD BOUNDARY. PhD Thesis. Technical University of Berlin.

Almond, D.C., Ahmed, F., 1987. Ductile shear zones in the northern Red Sea Hills, Sudan and their implication for crustal collision. Geological Journal 22, 175–184. https://doi.org/10.1002/gj.3350220614

Augustin, J., Gaboury, D., Crevier, M., 2017. Structural and gold mineralizing evolution of the world-class orogenic Mana district, Burkina Faso: Multiple mineralizing events over 150 million years. Ore Geology Reviews 91, 981–1012. https://doi.org/10.1016/j.oregeorev.2017.08.007

Bailo, T., Schandelmeier, H., Franz, G., Sun, C.-H., Stern, R.J., 2003. Plutonic and metamorphic rocks from the Keraf Suture (NE Sudan): a glimpse of Neoproterozoic tectonic evolution on the NE margin of W. Gondwana. Precambrian Research 123, 67–80. https://doi.org/10.1016/S0301-9268(03)00044-5

Bedeaux, P., Pilote, P., Daigneault, R., Rafini, S., 2017. Synthesis of the structural evolution and associated gold mineralization of the Cadillac Fault, Abitibi, Canada. Ore Geology Reviews 82, 49–69. https://doi.org/10.1016/j.oregeorev.2016.11.029

Bennett, J.D., Mosley, P.N., 1987. Tiered-tectonics and evolution, Eastern Desert and Sinai, Egypt. Colloquium on African Geology. 14. 79–82.

Berhe, S.M., 1990. Ophiolites in Northeast and East Africa: implications for Proterozoic crustal growth. Journal of the Geological Society 147, 41–57.

Bierlein, F.P., Groves, D.I., Goldfarb, R.J., Dubé, B., 2006. Lithospheric controls on the formation of provinces hosting giant orogenic gold deposits. Mineralium Deposita 40, 874–886. https://doi.org/10.1007/s00126-005-0046-2

Blewett, R.S., Czarnota, K., Henson, P.A., 2010. Structural-event framework for the eastern Yilgarn Craton, Western Australia, and its implications for orogenic gold. Precambrian Research 183, 203–229. https://doi.org/10.1016/j.precamres.2010.04.004

Bons, P.D., Elburg, M.A., Gomez-Rivas, E., 2012. A review of the formation of tectonic veins and their microstructures. Journal of Structural Geology 43, 33–62. https://doi.org/10.1016/j.jsg.2012.07.005

Botros, N.S., 2004. A new classifiaction of the gold deposits of Egypt. Ore Geology Reviews 25, 1–37.

Botros, N.S., 2002. Metallogeny of gold in relation to the evolution of the Nubian Shield in Egypt. Ore Geology Reviews 19, 137–164.

Burke, K., Sengör, C., 1986. Tectonic escape in the evolution of the continental crust. In: Barazangi, M., Brown, L. (Eds.), Geodynamics Series. American Geophysical Union, Washington, D. C., 41–53. https://doi.org/10.1029/GD014p0041

Chetty, T., 2017. Orogens. Proterozoic Orogens of India. Elsevier, 1–34. https://doi.org/10.1016/B978-0-12-804441-4.00001-8

Combes, V., Eglinger, A., André-Mayer, A.-S., Teitler, Y., Heuret, A., Gibert, P., Béziat, D., 2021. Polyphase gold mineralisation at the Yaou deposit, French Guiana. In: Torvela, T., Chapman, R.J., Lambert-Smith, J. (Eds.), Geological Society, London, Special Publications.

Cook, N.J., Chryssoulis, S.L., 1990. Concentrations of invisible gold in the common sulfides. The Canadian Mineralogist 28, 1–16.

Daigneault, R., Mueller, W.U., Chown, E.H., 2002. Oblique Archean subduction: accretion and exhumation of an oceanic arc during dextral transpression, Southern Volcanic Zone, Abitibi Subprovince Canada. Precambrian Research 115, 261–290.

Dawoud, A.S., 1980. Structural and metamorphic evolution of the area southwest of Abu Hamed, Nile Province, Sudan. Unpublished Ph. D Thesis, University of Khartoum.

Deditius, A.P., Reich, M., Kesler, S.E., Utsunomiya, S., Chryssoulis, S.L., Walshe, J., Ewing, R.C., 2014. The coupled geochemistry of Au and As in pyrite from hydrothermal ore deposits. Geochimica et Cosmochimica Acta 140, 644–670. https://doi.org/10.1016/j.gca.2014.05.045

Denkler, T., Franz, G., Schandelmeier, H., 1994. Tectonometamorphic evolution of the Neoproterozoic Delgo suture zone, northern Sudan. Geologische Rundschau 83, 578–590.

Denkler, T., Franz, G., Schandelmeier, H., Darbyshire, D.P.F., Harms, U., Pilot, J., 1993. Evolution of the south-western part of the Atmur-Delgo suture. Geoscientific Research in Northeast Africa. Balkema, Rotterdam Brookfield 87–89.

Domeier, M., Torsvik, T.H., 2014. Plate tectonics in the late Paleozoic. Geoscience Frontiers 5, 303–350.

Eglinger, A., André-Mayer, A.-S., Combes, V., Teitler, Y., Heuret, A., 2020. Les gisements d'or de la Guyane française. Géologues 206, 36–40.

Eglinger, A., Thébaud, N., Zeh, A., Davis, J., Miller, J., Parra-Avila, L.A., Loucks, R., McCuaig, C., Belousova, E., 2017. New insights into the crustal growth of the Paleoproterozoic margin of the Archean Kéména-Man domain, West African craton (Guinea): Implications for gold mineral system. Precambrian Research 292, 258–289. https://doi.org/10.1016/j.precamres.2016.11.012

Egyptian Geological Survey and Mining Authority, 1981. Geologic Map of Egypt., scale 1/2000000, Ministry of Industry and Mineral Resources - Egyptian Geological Survey and Mining Authority.

El Kazzaz, Y.A., 2012. Shear zones-related gold-bearing quartz veins in Shinai area, South eastern desert, Egypt. Egyptian Journal of Geology 56, 67–89.

Elsamani, Y., Almuslem, A.A., Tokhi, M.E., 2001. Geology and Geotectonic Classification of Pan-African Gold Mineralizations in the Red Sea Hills, Sudan. International Geology Review 43, 1117–1128. https://doi.org/10.1080/00206810109465064

Evuk, D., Franz, G., Frei, D., Lucassen, F., 2014. The Neoproterozoic evolution of the central-eastern Bayuda Desert (Sudan). Precambrian Research 240, 108–125. https://doi.org/10.1016/j.precamres.2013.10.015

Fawzy, K.M., 2017. Ore Mineralogical and Geochemical Studies on El-Daghbag-I Gold Deposit, Central Eastern Desert, Egypt. Open Journal of Geology 07, 395–419. https://doi.org/10.4236/ojg.2017.73027

Feybesse, J.-L., Billa, M., Guerrot, C., Duguey, E., Lescuyer, J.-L., Milesi, J.-P., Bouchot, V., 2006. The paleoproterozoic Ghanaian province: Geodynamic model and ore controls, including regional stress modeling. Precambrian Research 149, 149–196.

Fontaine, A., Dubé, B., Malo, M., Turcotte, J., Doucet, D., 2018. Geology of the Cheechoo gold property, Eeyou Istchee Baie-James, Superior Province, northern Quebec. No. 8403. https://doi.org/10.4095/308244

Fontaine, A., Eglinger, A., Ada, K., André-Mayer, A.-S., Reisberg, L., Siebenaller, L., Le Mignot, E., Ganne, J., Poujol, M., 2017. Geology of the world-class Kiaka polyphase gold deposit, West African Craton, Burkina Faso. Journal of African Earth Sciences 126, 96–122. https://doi.org/10.1016/j.jafrearsci.2016.11.017

Fossen, H., Cavalcante, G.C.G., Pinheiro, R.V.L., Archanjo, C.J., 2019. Deformation – Progressive or multiphase? Journal of Structural Geology 125, 82–99. https://doi.org/10.1016/j.jsg.2018.05.006

Frisch, W., Pohl, W., 1986. Petrochemistry of some mafic and ultramafic rocks from the Mozambique Belt, SE Kenya. Mitteilungen Der Osterreichischen Geologischen Gesellschaft 78, 97–114.

Fritz, H., Abdelsalam, M., Ali, K.A., Bingen, B., Collins, A.S., Fowler, A.R., Ghebreab, W., Hauzenberger, C.A., Johnson, P.R., Kusky, T.M., Macey, P., Muhongo, S., Stern, R.J., Viola, G., 2013. Orogen styles in the East African Orogen: A review of the Neoproterozoic to Cambrian tectonic evolution. Journal of African Earth Sciences 86, 65–106. https://doi.org/10.1016/j.jafrearsci.2013.06.004

Gaboury, D., Nabil, H., Ennaciri, A., Maacha, L., 2020. Structural setting and fluid composition of gold mineralization along the central segment of the Keraf suture, Neoproterozoic Nubian Shield, Sudan: implications for the source of gold. International Geology Review 1–27. https://doi.org/10.1080/00206814.2020.1838336

Geological Research Authority of the Sudan, 1988. Geological Map of the Sudan., scale 1/1000000, Robertson Research.

Goldfarb, R.J., André-Mayer, A.-S., Jowitt, S.M., Mudd, G.M., 2017. West Africa: The World's Premier Paleoproterozoic Gold Province. Economic Geology 112, 123–143. https://doi.org/10.2113/econgeo.112.1.123

Goldfarb, R.J., Baker, T., Dubé, B., Groves, D.I., Hart, C.J.R., Gosselin, P., 2005. Distribution, character and genesis of gold deposits in metamorphic terranes. Economic Geology 100th Anniversary Volume, 407–450.

Goldfarb, R.J., Groves, D.I., Gardoll, S., 2001. Orogenic gold and geologic time: a global synthesis. Ore Geology Reviews 18, 1–75.

Gray, D.R., Foster, D.A., Meert, J.G., Goscombe, B.D., Armstrong, R., Trouw, R.A.J., Passchier, C.W., 2008. A Damara orogen perspective on the assembly of southwestern Gondwana. Geological Society, London, Special Publications 294, 257–278.

Greiling, R.O., Abdeen, M.M., Dardir, A.A., El Akhal, H., El Ramly, M.F., Kamal, G.E.D., Osman, A.F., Rashwan, A.A., Rice, A.H.N., Sadek, M.F., 1994. A structural synthesis of the Proterozoic Arabian-Nubian Shield in Egypt. Geologische Rundschau 83, 484–501.

Greiling, R.O., Kroner, A., El-Ramly, M.F., Rashwan, A.A., 1988. Structural relationships between in the Southern and Central parts of the Eastern Desert of Egypt: details of a fold and thrust belt. The Pan-African Belt of Northeast Africa and Adjacent Areas: Tectonic Evolution and Economic Aspects of a Late Proterozoic Oregon. 121–145.

Grenholm, M., 2019. The global tectonic context of the ca. 2.27-1.96 Ga Birimian Orogen – Insights from comparative studies, with implications for supercontinent cycles. Earth-Science Reviews 193, 260–298. https://doi.org/10.1016/j.earscirev.2019.04.017

Groves, D.I., Goldfarb, R.J., Robert, F., Hart, C.J., 2003. Gold deposits in metamorphic belts: overview of current understanding, outstanding problems, future research, and exploration significance. Economic Geology 98, 1–29.

Groves, D.I., Santosh, M., Deng, J., Wang, Q., Yang, L., Zhang, L., 2019. A holistic model for the origin of orogenic gold deposits and its implications for exploration. Mineralium Deposita. https://doi.org/10.1007/s00126-019-00877-5

Groves, D.I., Santosh, M., Goldfarb, R.J., Zhang, L., 2018. Structural geometry of orogenic gold deposits: Implications for exploration of world-class and giant deposits. Geoscience Frontiers. https://doi.org/10.1016/j.gsf.2018.01.006

Harms, U., Darbyshire, D.P.F., Denkler, T., Hengst, M., Schandelmeier, H., 1994. Evolution of the Neoproterozoic Delgo suture zone and crustal growth in northern Sudan: geochemical and radiogenic isotope constraints. Geologische Rundschau 83, 591–603.

Helmy, H., Zoheir, B., 2015. Metal and fluid sources in a potential world-class gold deposit: El-Sid mine, Egypt. International Journal of Earth Sciences 104, 645–661. https://doi.org/10.1007/s00531-014-1094-6

Helmy, HassanM., Kaindl, R., Fritz, H., Loizenbauer, J., 2004. The Sukari GoldCo Mine, Eastern Desert, Egypt: structural setting, mineralogy and fluid inclusion study. Mineralium Deposita 39. https://doi.org/10.1007/s00126-004-0426-z

Hough, R.M., Noble, R.R.P., Reich, M., 2011. Natural gold nanoparticles. Ore Geology Reviews 42, 55–61. https://doi.org/10.1016/j.oregeorev.2011.07.003

Johnson, P.R., Andresen, A., Collins, A.S., Fowler, A.R., Fritz, H., Ghebreab, W., Kusky, T., Stern, R.J., 2011. Late Cryogenian–Ediacaran history of the Arabian–Nubian Shield: A review of depositional, plutonic, structural, and tectonic events in the closing stages of the northern East African Orogen. Journal of African Earth Sciences 61, 167–232. https://doi.org/10.1016/j.jafrearsci.2011.07.003

Johnson, P.R., Zoheir, B.A., Ghebreab, W., Stern, R.J., Barrie, C.T., Hammer, R.D., 2017. Gold-bearing volcanogenic massive sulfides and orogenic-gold deposits in the Nubian Shield. South African Journal of Geology 120, 63–76.

Kerrich, R., Wyman, D., 1990. Geodynamic setting of mesothermal gold deposits: An association with accretionary tectonic regimes. Geology 18, 882. https://doi.org/10.1130/0091-7613(1990)018<0882:GSOMGD>2.3.CO;2

Khalil, K.I., Moghazi, A.M., El Makky, A.M., 2016. Nature and Geodynamic Setting of Late Neoproterozoic Vein-Type Gold Mineralization in the Eastern Desert of Egypt: Mineralogical and Geochemical Constraints. In: Bouabdellah, M., Slack, J.F. (Eds.), Mineral Deposits of North Africa. Springer International Publishing, Cham, 353–370. https://doi.org/10.1007/978-3-319-31733-5_14

Klemm, D., Klemm, R., Murr, A., 2001. Gold of the Pharaohs – 6000 years of gold mining in Egypt and Nubia. Journal of African Earth Sciences 33, 643–659. https://doi.org/10.1016/S0899-5362(01)00094-X

Kröner, A., 1993. The Pan African belt of northeastern and eastern Africa, Madagascar, southern India, Sri Lanka and East Antarctica: Terrane amalgamation during formation of the Gondwana supercontinent. In: Thorweihe, U., Schandelmeier, H. (Eds.), Geoscientific Research in Northeast Africa. CRC Press, 3–9.

Kusky, T.M., Abdelsalam, M., Tucker, R.D., Stern, R.J., 2003. Evolution of the East African and related orogens, and the assembly of Gondwana. Precambrian Research 123, 81–85. https://doi.org/10.1016/S0301-9268(03)00062-7

Le Mignot, E., Reisberg, L., André-Mayer, A.-S., Bourassa, Y., Fontaine, A., Miller, J., 2017. Re-Os Geochronological Evidence for Multiple Paleoproterozoic Gold Events at the Scale of the West African Craton. Economic Geology 112, 145–168. https://doi.org/10.2113/econgeo.112.1.145

Li, Z.X., Bogdanova, S.V., Collins, A.S., Davidson, A., De Waele, B., Ernst, R.E., Fitzsimons, I.C.W., Fuck, R.A., Gladkochub, D.P., Jacobs, J., Karlstrom, K.E., Lu, S., Natapov, L.M., Pease, V., Pisarevsky, S.A., Thrane, K., Vernikovsky, V., 2008. Assembly, configuration, and break-up history of Rodinia: A synthesis. Precambrian Research 160, 179–210. https://doi.org/10.1016/j.precamres.2007.04.021

Managem, 2014. Exploration activities in Sudan.

Managem, 2011. Exploration activities in Sudan.

Masurel, Q., Eglinger, A., Thébaud, N., Allibone, A., André-Mayer, A.-S., McFarlane, H., Miller, J., Jessell, M., Aillères, L., Vanderhaeghe, O., Salvi, S., Baratoux, L., Perrouty, S., Begg, G., Fougerouse, D., Hayman, P., Wane, O., Tshibubudze, A., Parra-Avila, L., Kouamélan, A., Amponsah, P.O., 2021. Paleoproterozoic gold events in the southern West African Craton: review and synopsis. Mineralium Deposita. https://doi.org/10.1007/s00126-021-01052-5

Meinhold, K.D., 1979. The Precambrian basement complex of the Bayuda Desert, northern Sudan.

Merdith, A.S., Collins, A.S., Williams, S.E., Pisarevsky, S., Foden, J.D., Archibald, D.B., Blades, M.L., Alessio, B.L., Armistead, S., Plavsa, D., Clark, C., Müller, R.D., 2017. A full-plate global reconstruction of the Neoproterozoic. Gondwana Research 50, 84–134. https://doi.org/10.1016/j.gr.2017.04.001

Mole, D.R., Kirkland, C.L., Fiorentini, M.L., Barnes, S.J., Cassidy, K.F., Isaac, C., Belousova, E.A., Hartnady, M., Thebaud, N., 2019. Time-space evolution of an Archean craton: A Hf-isotope window into continent formation. Earth-Science Reviews 196, 102831. https://doi.org/10.1016/j.earscirev.2019.04.003

Mosley, P.N., 1993. Geological evolution of the late Proterozoic "Mozambique Belt" of Kenya. Tectonophysics 221, 223–250.

Mueller, A.G., 2017. Structural setting of Fimiston- and Oroya-style pyrite-telluride-gold lodes, Paringa South mine, Golden Mile, Kalgoorlie: 1. Shear zone systems, porphyry dykes and deposit-scale alteration zones. Mineralium Deposita. https://doi.org/10.1007/s00126-017-0747-3

Mueller, A.G., Hagemann, S.G., McNaughton, N.J., 2016. Neoarchean orogenic, magmatic and hydrothermal events in the Kalgoorlie-Kambalda area, Western Australia: constraints on gold mineralization in the Boulder Lefroy-Golden Mile fault system. Mineralium Deposita. https://doi.org/10.1007/s00126-016-0665-9

Osman, A.E.M., 2014. An integrated metallotect and petrographic model for gold mineralization in the Eastern Desert of Egypt; a new prospecting vision. Journal of Egyptian Pure and Applied Sciences 52, 41–54.

Passchier, C.W., Trouw, R.A.J., 2005. Microtectonics, 2nd edition. ed. Springer, Berlin, New-York.

Perret, J., Eglinger, A., André-Mayer, A.-S., Aillères, L., Feneyrol, J., Hartshorne, C., Abanyin, E., Bosc, R., 2020. Subvertical, linear and progressive deformation related to gold mineralization at the Galat Sufar South deposit, Nubian Shield, NE Sudan. Journal of Structural Geology 135. https://doi.org/10.1016/j.jsg.2020.104032

Pokrovski, G.S., Kokh, M.A., Proux, O., Hazemann, J.-L., Bazarkina, E.F., Testemale, D., Escoda, C., Boiron, M.-C., Blanchard, M., Aigouy, T., Gouy, S., de Parseval, P., Thibaut, M., 2019. The nature and partitioning of invisible gold in the pyrite-fluid system. Ore Geology Reviews 109, 545–563. https://doi.org/10.1016/j.oregeorev.2019.04.024

Rabeau, O., Royer, J.-J., Jébrak, M., Cheilletz, A., 2013. Log-uniform distribution of gold deposits along major Archean fault zones. Mineralium Deposita 48, 817–824. https://doi.org/10.1007/s00126-013-0470-7

Reich, M., Kesler, S.E., Utsunomiya, S., Palenik, C.S., Chryssoulis, S.L., Ewing, R.C., 2005. Solubility of gold in arsenian pyrite. Geochimica et Cosmochimica Acta 69, 2781–2796. https://doi.org/10.1016/j.gca.2005.01.011

Ries, A.C., Shackleton, R.M., Dawoud, A.S., 1985. Geochronology, geochemistry and tectonics of the NE Bayuda Desert, N Sudan: Implications for the western margin of the late Proterozoic fold belt of NE Africa. Precambrian Research 30, 43–62. https://doi.org/10.1016/0301-9268(85)90028-2

Ries, A.C., Shackleton, R.M., Graham, R.H., Fitches, W.R., 1983. Pan-African structures, ophiolites and mélange in the Eastern Desert of Egypt: a traverse at 26 N. Journal of the Geological Society 140, 75–95.

Ries, A.C., Vearncombe, J.R., Price, R.C., Shackleton, R.M., 1992. Geochronology and geochemistry of the rocks associated with a late Proterozoic ophiolite in West Pokot, NW Kenya. Journal of African Earth Sciences (and the Middle East) 14, 25–35.

Rutter, E.H., 1986. On the nomenclature of mode of failure transitions in rocks. Tectonophysics 122, 381–387. https://doi.org/10.1016/0040-1951(86)90153-8

Sawkins, F.J., 1990. Metal Deposits in Relation to Plate Tectonics. Springer Berlin, Berlin.

Schandelmeier, H., Wipfler, E., Küster, D., Sultan, M., Becker, R., Stern, R.J., Abdelsalam, M.G., 1994. Atmur-Delgo suture: A Neoproterozoic oceanic basin extending into the interior of northeast Africa. Geology 22, 563. https://doi.org/10.1130/0091-7613(1994)022<0563:ADSANO>2.3.CO;2

Seton, M., Müller, R.D., Zahirovic, S., Gaina, C., Torsvik, T., Shephard, G., Talsma, A., Gurnis, M., Turner, M., Maus, S., 2012. Global continental and ocean basin reconstructions since 200 Ma. Earth-Science Reviews 113, 212–270.

Shackleton, R.M., 1986. Precambrian collision tectonics in Africa. Geological Society, London, Special Publications 19, 329–349.

Shackleton, R.M., Ries, A.C., 1984. The relation between regionally consistent stretching lineations and plate motions. Journal of Structural Geology 6, 111–117.

Shackleton, R.M., Ries, A.C., Graham, R.H., Fitches, W.R., 1980. Late Precambrian ophiolitic melange in the Eastern Desert of Egypt. Nature 285, 472–474.

Simard, M., Gaboury, D., Daigneault, R., Mercier-Langevin, P., 2013. Multistage gold mineralization at the Lapa mine, Abitibi Subprovince: insights into auriferous hydrothermal and metasomatic processes in the Cadillac–Larder Lake Fault Zone. Mineralium Deposita 48, 883–905. https://doi.org/10.1007/s00126-013-0466-3

Snoke, A.W., Tullis, J., Todd, V.R., 1998. The Princeton Atlas of Fault-related Rocks. Princeton University Press.

Stern, R.J., 1994. Arc Assembly and Continental Collision in the Neoproterozoic East African Orogen: Implications for the Consolidation of Gondwanaland. Annual Review of Earth and Planetary Sciences 22, 319–351. https://doi.org/10.1146/annurev.ea.22.050194.001535

Stern, R.J., Abdelsalam, M.G., Schandelmeier, H., Sultan, M., Wickham, S., 1993. Carbonates of the Keraf Zone, NE Sudan; a Neoproterozoic (ca. 750Ma) passive margin on the eastern flank of West Gondwanaland. Geological Society of America Annual Meeting, Abstracts with Programs. A49.

Stern, R.J., Kröner, A., Bender, R., Reischmann, T., Dawoud, A.S., 1994. Precambrian basement around Wadi Haifa, Sudan: a new perspective on the evolution of the East Saharan Craton. Geologische Rundschau 83, 564–577.

Sturchio, N., Sultan, M., Sylvester, P., Batiza, R., Hedge, C., 1984. Geology, age, and origin of the Meatiq Dome: implications for the Precambrian stratigraphy and tectonic evolution of the Eastern Desert of Egypt.

Tadesse, S., Milesi, J.-P., Deschamps, Y., 2000. Geology and Mineral Map of Ethiopia., scale 1/2000000.

Thébaud, N., Allibone, A., Masurel, Q., Eglinger, A., Davis, J., André-Mayer, A.-S., Miller, J., Ouedrago, M.F., Jessell, M., 2020. Chapter XX The Paleoproterozoic (Rhyacian) Gold Deposits of West Africa. Society of Economic Geologist, Special Publication 18.

Tikoff, B., Blenkinsop, T., Kruckenberg, S.C., Morgan, S., Newman, J., Wojtal, S., 2013. A perspective on the emergence of modern structural geology: Celebrating the feedbacks between historical-based and process-based approaches. The Web of Geological Sciences: Advances, Impacts, and Interactions. Geological Society of America. https://doi.org/10.1130/2013.2500(03)

Turlin, F., Jébrak, M., De Souza, S., Turcotte, J., 2019. Topological characterization of a polyphased gold-bearing vein network. Journal of Structural Geology 128, 103872. https://doi.org/10.1016/j.jsg.2019.103872

Twiss, R.J., Moores, E.M., 2007. Structural Geology. © WH Freeman and Company. New York 532.

Vail, J.R., 1985. Pan-African (late Precambrian) tectonic terrains and the reconstruction of the Arabian-Nubian Shield. Geology 13, 839. https://doi.org/10.1130/0091-7613(1985)13<839:PLPTTA>2.0.CO;2

Vail, J.R., 1983. Pan-African crustal accretion in north-east Africa. Journal of African Earth Sciences (1983) 1, 285–294. https://doi.org/10.1016/S0731-7247(83)80013-5

Vail, J.R., 1979. Outline of geology and mineralization of the Nubian Shield east of the Nile valley, Sudan In: Tahon, S> A>,(ed.). Evolution and mineralization of the Arabian Nu bian Shield, 1, 97-107. Pergamon press.

Vearncombe, J.R., 1983. A dismembered ophiolite from the Mozambique belt, west Pokot, Kenya. Journal of African Earth Sciences (1983) 1, 133–143.

Weinberg, R.F., Hodkiewicz, P.F., Groves, D.I., 2004. What controls gold distribution in Archean terranes? Geology 32, 545. https://doi.org/10.1130/G20475.1

Weinberg, R.F., Van der Borgh, P., Bateman, R.J., Groves, D.I., 2005. Kinematic history of the Boulder-Lefroy shear zone system and controls on associated gold mineralization, Yilgarn Craton, Western Australia. Economic Geology 100, 1407–1426.

Zoheir, B., Emam, A., Soliman, N., Holzheid, A., 2019a. Gold Metallogeny of the Egyptian South Eastern Desert. Springer Berlin Heidelberg, Berlin, Heidelberg, 261–263. https://doi.org/10.1007/978-3-030-01575-6_63

Zoheir, B., Steele-MacInnis, M., Garbe-Schönberg, D., 2019b. Orogenic gold formation in an evolving, decompressing hydrothermal system: Genesis of the Samut gold deposit, Eastern Desert, Egypt. Ore Geology Reviews 105, 236–257. https://doi.org/10.1016/j.oregeorev.2018.12.030